

Contents lists available at [ScienceDirect](https://www.sciencedirect.com)

Journal of Rock Mechanics and Geotechnical Engineering

journal homepage: www.jrmge.cn

Full Length Article

Assessment of cyclic deformation and critical stress amplitude of jointed rocks via cyclic triaxial testing

Waranga Habaraduwa Peellage, Behzad Fatahi*, Haleh Rasekh

School of Civil and Environmental Engineering, University of Technology Sydney, Sydney, Australia

ARTICLE INFO

Article history:

Received 18 May 2022

Received in revised form

13 November 2022

Accepted 6 February 2023

Available online xxx

Keywords:

Cyclic triaxial test

Jointed rock

Joint surface

Confining pressure

Cyclic deviatoric stress amplitude

Failure

Residual deformation

Dissipated energy

ABSTRACT

Jointed rock specimens with a natural replicated joint surface oriented at a mean dip angle of 60° were prepared, and a series of cyclic triaxial tests was performed at different confining pressures and cyclic deviatoric stress amplitudes. The samples were subjected to 10,000 loading-unloading cycles with a frequency of 8 Hz. At each level of confining pressure, the applied cyclic deviatoric stress amplitude was increased incrementally until excessive deformation of the jointed rock specimen was observed. Analysis of the test results indicated that there existed a critical cyclic deviatoric stress amplitude (i.e. critical dynamic deviatoric stress) beyond which the jointed rock specimens yielded. The measured critical dynamic deviatoric stress was less than the corresponding static deviatoric stress. At cyclic deviatoric stress amplitudes less than the critical dynamic deviatoric stress, minor cumulative residual axial strains were observed, resulting in hysteretic damping. However, for cyclic deviatoric stresses beyond the critical dynamic deviatoric stress, the plastic strains increased promptly, and the resilient moduli degraded rapidly during the initial loading cycles. Cyclic triaxial test results showed that at higher confining pressures, the ultimate residual axial strain attained by the jointed rock specimen decreased, the steady-state dissipated energy density and steady-state damping ratio per load cycle decreased, while steady-state resilient moduli increased.

© 2023 Institute of Rock and Soil Mechanics, Chinese Academy of Sciences. Production and hosting by Elsevier B.V. This is an open access article under the CC BY-NC-ND license (<http://creativecommons.org/licenses/by-nc-nd/4.0/>).

1. Introduction

In foundation design, avoiding excessive deformation under the applied loads is one of the key performance requirements evaluated by engineers (Craig, 2004). The Leaning Tower of Pisa is a classic example that points out the significance of evaluating deformation characteristics of the ground precisely at the design phase. The deformation response of the ground under static loading conditions has been extensively studied and reported in the literature. However, soil and rock formations are often subjected to cyclic loads generated through natural causes such as earthquakes, wave actions, landslides and volcanic eruptions and human activities such as construction and demolition activities, traffic loads and machine vibrations (Sheng et al., 2006; Huang et al., 2007). It is well established that the material behaviour under cyclic loading is highly different from that under static loading. Under extreme

conditions, cyclic loading may induce instantaneous settlements, leading to instability, damage and even disastrous failure in structures (Prakash, 1981; Yasuhara et al., 2001; Das and Ramana, 2011).

According to Ng et al. (2013), cyclic loading due to running trains was considered as one of the possible causes of excessive long-term tunnel settlements observed along several metro lines in Shanghai. Shi et al. (2014) reported that a large number of rail tracks had been built on or across soft rocks in China, which had resulted in problems such as accumulated deformation and settlements in the tracks jeopardising the safety and efficiency of train operations. Rainer (1982) reported that foundation settlements were observed even in buildings far from railway lines inducing continuous vibrations over extended periods of loading. Lacy and Gould (1985) analysed cases of damage to nearby structures caused by settlement from pile driving and concluded that increasing cyclic loading induced by pile driving could lead to damaging levels of settlements. According to Yasuhara et al. (2001), extreme destruction was experienced in the 1957 and 1985 earthquakes in Mexico and the 1964 earthquake in Alaska due to seismically induced differential settlements. Massive land and rock slides triggered by the 1999 earthquake in central Taiwan (Chen et al., 2004), the 2002

* Corresponding author.

E-mail address: behzad.fatahi@uts.edu.au (B. Fatahi).

Peer review under responsibility of Institute of Rock and Soil Mechanics, Chinese Academy of Sciences.

<https://doi.org/10.1016/j.jrmge.2023.02.001>

1674-7755 © 2023 Institute of Rock and Soil Mechanics, Chinese Academy of Sciences. Production and hosting by Elsevier B.V. This is an open access article under the CC BY-NC-ND license (<http://creativecommons.org/licenses/by-nc-nd/4.0/>).

Alaska earthquake (Jibson et al., 2006) and the 2008 Wenchuan earthquake (Qi et al., 2011) can be considered as well documented case histories for catastrophic events due to seismically induced deformation of fractured and weak rock blocks.

Therefore, it is of utmost significance to evaluate the deformation behaviour of grounds subjected to dynamic loads during the design phase of structures rigorously. Yet, research studies on deformation characteristics and the evolution process of deformation of rock masses, particularly jointed rock masses subjected to cyclic loading, are scarce. Rock masses present in nature generally consist of discontinuities such as joints, fractures, and other planes of weakness. The presence of such discontinuities significantly influences the strength and deformability of rock masses (Huang et al., 1993; Xie et al., 1997; Belem et al., 2007). According to Hungr and Coates (1978), settlement predictions are of paramount importance for structures founded on the jointed rock since joint deformation can constitute a major part of the settlement of the rock stratum. Huang et al. (1993) stated that during excavations and constructions at shallow depths of rock masses, the deformation of the rock mass is primarily controlled by the joint behaviour. Therefore, it is important to study the deformation behaviour of jointed rocks subjected to cyclic loading.

In the past few decades, many researchers have carried out experimental and theoretical studies to investigate the deformation response of various intact rock types subjected to cyclic loading under uniaxial or triaxial conditions. The effect of cyclic loading on the dynamic strength and deformation characteristics of various intact rocks and their evolution in terms of loading amplitude (Attewell and Farmer, 1973; Tao and Mo, 1990; Bagde and Petros, 2005a; Bagde and Petros, 2009; Ma et al., 2013; Momeni et al., 2015), frequency (Attewell and Farmer, 1973; Bagde and Petros, 2005a; Bagde and Petros, 2009; Liu et al., 2012; Ma et al., 2013) and waveform (Tao and Mo, 1990; Bagde and Petros, 2005b) were also studied. Apart from the studies mentioned above, which were carried out under constant cyclic loading amplitude, some experimental investigations were also conducted with variable cyclic loading amplitudes (i.e. stepwise increasing amplitudes, multi-level cyclic loading and random cyclic loading) (Liang et al., 2012; Jia et al., 2018; Vaneghi et al., 2018; Peng et al., 2019; Liu et al., 2021a). Researchers also defined numerous damage parameters to describe the dynamic damage evolution and failure of various intact rocks under cyclic loading conditions (Xiao et al., 2009, 2010; Liu et al., 2011; Liu and He, 2012; Li et al., 2019). In addition, researchers employed energy theories and principles to analyse the energy dissipation mechanism that governs the deformation and failure of different intact rocks under cyclic loading (Bagde and Petros, 2009; Yang et al., 2016; Zhang et al., 2017; Song et al., 2020; He et al., 2021).

Moreover, several researchers executed systematic experimental and theoretical studies to investigate the jointed rock behaviour under cyclic loading conditions. Most of these scholars conducted cyclic direct shear tests to investigate the shearing mechanism, dilation and asperity degradation behaviour under cyclic shearing. They also analysed the influence of joint asperity characteristics, loading rate, number of cycles and normal stress on the jointed rock behaviour under cyclic direct shear loading (Hutson and Dowding, 1990; Huang et al., 1993; Lee et al., 2001; Jafari et al., 2003; Belem et al., 2007; Zheng and Qi, 2016; Fathi et al., 2016; Niktabar et al., 2017; Kou et al., 2019).

In addition, a few researchers carried out experimental and theoretical investigations to study the response of jointed rocks subjected to cyclic uniaxial or triaxial loading conditions. Early studies on intermittently jointed rock samples conducted by Brown and Hudson (1973) and Li et al. (2001a, b) under cyclic uniaxial loading conditions and Prost (1988) under cyclic triaxial loading

conditions assessed the effect of cyclic loading on the dynamic strength and deformation of intermittent joints. Later, Liu et al. (2017, 2018a, b) conducted cyclic uniaxial compression tests on intermittently jointed rock samples and further analysed deformation characteristics, energy evolution, fatigue damage and failure modes of intermittent joints under cyclic uniaxial compression. Jafari et al. (2003, 2004) investigated the effect of cyclic loading (i.e. number of cycles and cyclic stress amplitude) on the shear strength of saw-toothed rock joint samples under triaxial conditions. Ding et al. (2014) studied the effect of contact condition of joints on the deformation behaviour of rocks under cyclic triaxial loading. Studies by Liu and Liu (2017) and Zheng et al. (2020a, b) investigated the deformation characteristics, dynamic damage and failure mechanism of prefabricated jointed rock with a planar joint surface under cyclic triaxial conditions. They also defined damage variables capturing the dynamic damage evolution of the jointed rock samples. Later, Peellage et al. (2022) explored the deformation behaviour and energy characteristics of jointed rocks with planar, sawtooth and natural replicated joint surfaces by performing cyclic triaxial tests under train loading conditions.

Indeed, most of the previous research studies on rocks under cyclic loading conditions had focused on the deformation response and dynamic properties of intact rocks. However, only a few research studies are available related to the jointed rock behaviour under cyclic loading conditions. Among the available studies on the cyclic behaviour of jointed rocks, most studies have utilised cyclic direct shear apparatus for continuous penetrating joints and used cyclic triaxial or uniaxial apparatus for prefabricated intermittent joints. Experimental studies on jointed rocks with continuous penetrating joints replicating a natural rough joint surface under cyclic triaxial conditions are rather scarce. In the meantime, the deformation behaviour and dynamic characteristics of jointed rocks under cyclic loadings in terms of deformation characteristics and yielding, energy and damage evolution and damping characteristics were not investigated rigorously in the past. Therefore, this study experimentally investigates the deformation response and dynamic mechanical characteristics of jointed rock specimens with a natural joint surface subjected to cyclic triaxial test conditions. Indeed, this study provides an important reference and quantifies variations of parameters such as permanent deformation, yielding stress, stiffness and damping ratio with field conditions. Design engineers can use results of this study for more reliable predictions of response of jointed rock subjected to cyclic loading and efficient and cost-effective solutions to curtail excessive deformation of structures built on or near jointed rock foundations subjected to cyclic loading from machine foundations, railway, road traffic loads and rock cutting. The cyclic triaxial tests were conducted on replicated jointed rock samples with a natural joint surface oriented at a mean dip angle of 60° under different confining pressures and cyclic deviatoric stress amplitudes. The cyclic stress-strain response, yield stress, residual axial deformation evolution, stiffness degradation, dissipated energy evolution, and damping characteristics were analysed and discussed in detail.

2. Laboratory investigation

2.1. Sample preparation

The deformation behaviour of jointed rock was studied through a comprehensive laboratory test series conducted on a set of modelled rock joints having a natural joint surface. Due to the difficulty of obtaining a set of natural rock joints with the same morphology, replicas of jointed rock specimens can be cast with natural and synthetic materials. Stimpson (1970) provided a comprehensive summary of different types of model material used

to simulate rock for a variety of investigations. Gypsum plaster is one such material most commonly used to model different rock types, including sedimentary rocks (Hobbs, 1966; Rosenblad, 1971; Indraratna, 1990; Waltham and Swift, 2004; Atapour and Moosavi, 2014; Jahanian and Sadaghiani, 2015; Gong et al., 2018). It can also be moulded into various shapes and dries quickly with minimum apparent long-term changes in strength. In this study, gypsum plaster ($\text{CaSO}_4 \cdot \text{H}_2\text{O}$ hemihydrates, 98%) was used to make replicas of rock joints with a natural joint surface.

The cylindrical jointed rock specimens had a diameter of 50 mm and an overall height of 100 mm when the two halves of the specimen were fully mated. Hence, the jointed rock specimen maintained a height to diameter ratio of two as required for triaxial testing. According to Goodman (1989), when the joint is oriented at an angle 50° – 65° with the direction of minor principal stress, the joint will slip before fracturing the rock, allowing determination of the joint characteristics. According to Jafari et al. (2004) and Abdellah et al. (2016), the critical orientation of the joint can also be determined from the Mohr-Coulomb criterion given by $45^\circ + \phi/2$, where ϕ is the friction angle of the joint. Accordingly, in this study, the joint surface was oriented at 60° with the direction of minor principal stress.

Each side of the joint surface was cast separately to ensure that the joint was fully mated after assembly. To cast replicas of cylindrical jointed rock specimen, a cylindrical hollow mould and cylindrical moulds with each side of the natural joint surface were required. As reported by Peellage et al. (2022), cylindrical hollow moulds, 50 mm in diameter and 100 mm in height (see Fig. 1a), were created using acetal plastic since this material could be machined to obtain the desired shape. An actual block of sandstone taken from Kangaroo Valley, New South Wales, Australia, was split

to obtain a naturally rough rock surface, and Dlachem SRT30 mould making silicon rubber (in the liquid form) was used to copy the split sandstone rough surface to prepare moulds of each side of the joint surface (see Fig. 1b). This material consisted of a base component and a catalyst which were mixed in the ratio of 20:1 and poured over the split sandstone surface and allowed to harden. The rubber moulds were taken out after a setting time of 72 h and were used to cast the 50 mm diameter jointed cylindrical specimen. Then, the rubber moulds of the joint profiles were placed separately in cylindrical hollow moulds (Fig. 1c), and a silicon-based lubricant was sprayed on the joint surface and the interior wall of the hollow moulds to prevent the gypsum plaster mixture from adhering to the moulds. Gypsum cement was then mixed with water in the ratio of 3.5:1 by weight and stirred until it became a uniform mixture. The uniform mixture was then poured into the hollow moulds, and a mild vibration was applied to the moulds externally to release any air bubbles trapped in the gypsum mixture. After completion of the initial setting time of 30 min, the specimens (Fig. 1d) were removed from the moulds and cured for 2 weeks at a controlled temperature of 40°C . After the completion of curing time, the jointed specimens were used for testing after reaching room temperature. A comparable sample preparation procedure was reported by Peellage et al. (2022). Furthermore, three additional samples without a joint having 50 mm diameter and 100 mm height as reference samples were also prepared to determine the unconfined compressive and tensile strengths and the relevant values are summarised in Table 1.

2.2. Testing procedure

In this study, the triaxial setup was selected to perform all the tests since it is possible to model jointed rock specimens in a state similar to their real underground conditions during cyclic loading (Jafari et al., 2004; Peellage et al., 2022). In order to carry out the experimental work, the GDS ELDYN triaxial apparatus, as shown in Fig. 2a, was used when testing jointed rock samples under lower cyclic deviatoric stress amplitudes ($q_{\text{cyc}} < 400$ kPa) and a triaxial condition setup using the CMA electro-hydraulic actuator (Fig. 2b) was used when testing jointed rock samples subjected to higher cyclic deviatoric stress amplitudes ($q_{\text{cyc}} > 400$ kPa). In the ELDYN triaxial apparatus, the axial load was applied via the electro-mechanical actuator, which had a load capacity of 10 kN and a maximum frequency of 10 Hz could be applied, whereas the CMA electro-hydraulic actuator had a load capacity of 40 kN and a maximum frequency of 40 Hz could be applied. In both setups, the confining pressure was applied by pressurising the cell with de-aired water, which was controlled by air through the air pressure controller. After thorough checks and calibrations of the apparatus, the jointed rock specimen was placed on the triaxial base and then covered with a membrane and O-rings to seal the sample.

The tested samples had a natural replicated joint surface with a joint roughness coefficient (JRC) of 11.51. It should be noted that the JRC value of the joint surface was calculated using the relationships proposed by Tse and Cruden (1979) as follows:

Table 1
Mechanical properties of the hardened gypsum plaster mixture utilised to prepare natural replicated jointed specimens.

Property	Unit	Value
Basic friction angle, ϕ_b	$^\circ$	30
Uniaxial compressive strength, σ_c	MPa	62
Young's modulus, E_f	GPa	19
Tensile strength, σ_t	MPa	15

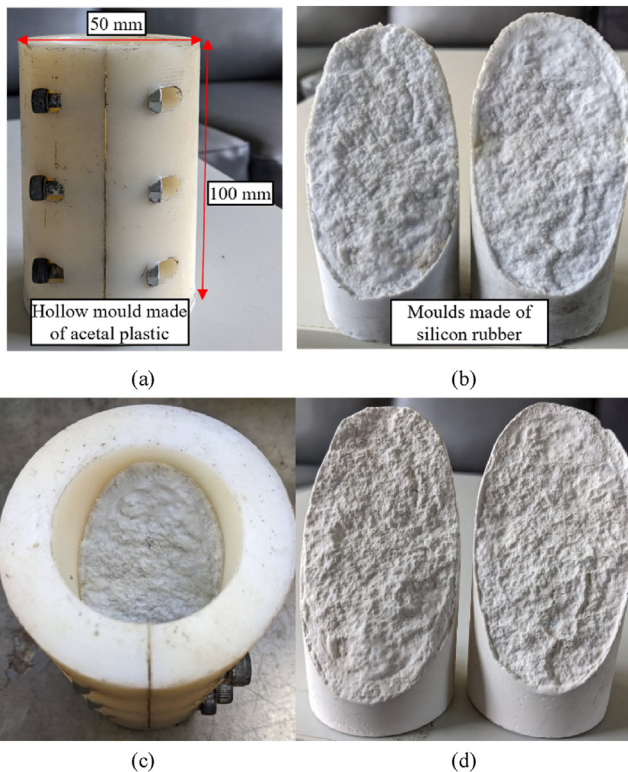


Fig. 1. (a) The transverse view of the cylindrical hollow mould, (b) Rubber moulds of the two opposite sides of the natural replicated joint surface, (c) The top view of the cylindrical hollow mould with one half of the joint mould inside it, and (d) The two opposite surfaces of a natural replicated jointed sample.

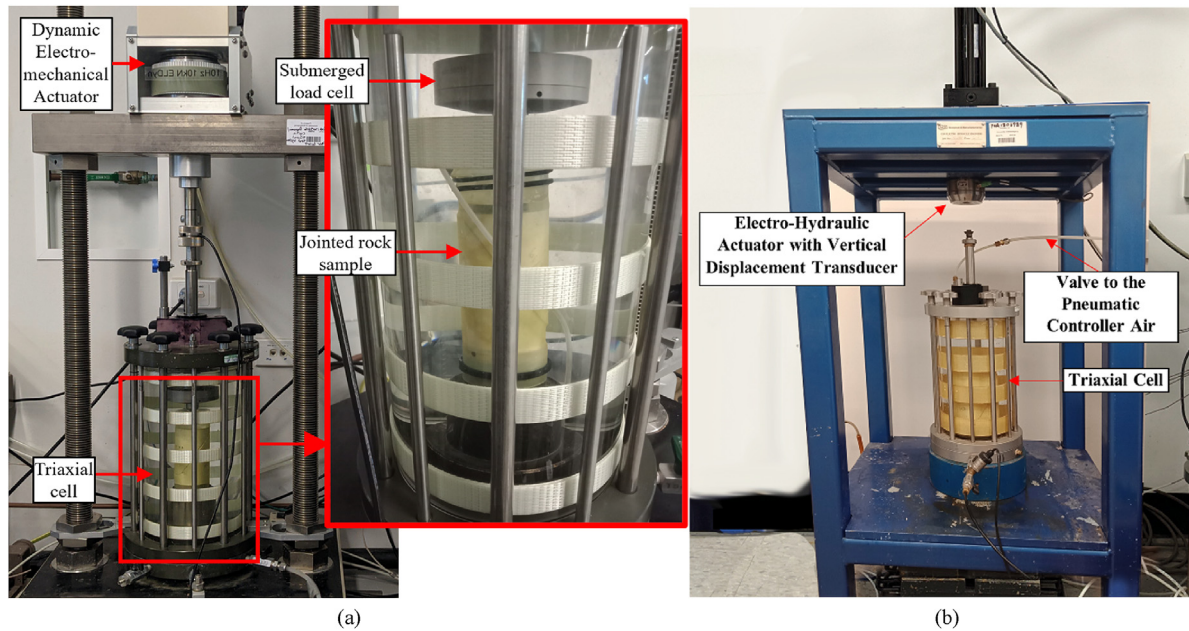


Fig. 2. (a) GDS 10 Hz cyclic triaxial equipment used in this study, and (b) Triaxial condition set up using the CMA electro-hydraulic actuator.

$$JRC = 32.2 + 32.47 \log_{10} Z_2 \quad (1)$$

where Z_2 is the root mean square of the first derivative of the profile which is given by

$$Z_2 = \sqrt{\frac{1}{L_n} \sum_{i=1}^{N_p-1} \frac{(Z_{i+1} - Z_i)^2}{x_{i+1} - x_i}} \quad (2)$$

where the values (x_i, z_i) and (x_{i+1}, z_{i+1}) represent the adjacent digitised coordinates of the profile separated by the sampling interval Δx , N_p is the number of digitised points along the profile, and L_n is the nominal length of the digitised joint profile. A non-contact three-dimensional (3D) digitiser (MINOLTA VIVID 910) was used for digitising the joint surface (Fig. 3). The digitised coordinates of 10 joint profiles along the shear direction of the joint surface were used to determine the weighted average JRC based on the coverage area to describe the roughness of the joint surface. Moreover, conventional static triaxial tests were conducted with a shearing rate of 0.05 mm/min to measure the friction angle of the joint ($\phi = 51^\circ$).

Six levels of confining pressures (i.e. 15 kPa, 20 kPa, 25 kPa, 90 kPa, 120 kPa and 150 kPa) were selected for the testing, in line with previous research studies by other researchers for laboratory testing, field measurements and numerical simulations of shallow rock formations for various applications. For examples, Sinha and Singh (2000) used an effective confining pressure of 125 kPa when simulating rock joints filled along the surface of the discontinuity in a rock mass prone to landslides. Liu and Liu (2017) simulated jointed rock masses subjected to cyclic loads such as seismic loads, train loads and blasting loads, using confining pressures in the range of 100–400 kPa. Ding et al. (2014) conducted cyclic triaxial tests with confining pressure of 200 kPa when analysing the stability of tunnel bed under high-speed train operation. Nie et al. (2020), Wang and Zhuang (2021) and Peellage et al. (2022) used confining pressures in the range of 20–150 kPa when simulating railway subgrades under train loads. In line with previous research studies, different cyclic deviatoric stress amplitudes were

used for each confining pressure in order to clearly identify the critical dynamic deviatoric stress. It should be noted that for each case with different cyclic deviatoric stress amplitude, a new jointed rock sample was used to ensure that micro-cracking from the previous loading amplitudes would not accumulate and impact the accurate determination of the critical dynamic stress.

In this study, the tests were terminated when 10,000 cycles of loading were applied. The minimum deviatoric stress was maintained, and the maximum deviatoric stress was adjusted to apply the target cyclic deviatoric stress amplitudes. The sinusoidal waveform was utilised to apply the cyclic load on the jointed rock samples. Frequencies in the range of 0.1–20 Hz were utilised in the past by previous researchers for cyclic tests simulating rock formations under dynamic loads such as earthquakes, construction and demolition activities, traffic loads and machine vibrations (Liu and Dai, 2021). For examples, Attewell and Farmer (1973) simulated rock engineering operations such as drilling for explosive blasting and cutting during tunnel boring, using frequencies in the range of 0.3–20 Hz. Bagde and Petros (2005a) used frequencies in the range of 0.1–10 Hz stimulating rockbursts. Liu et al. (2018a, b) simulated earthquake, quarrying and rockbursts using frequencies in the range 1–10 Hz. Referring to previous studies (Bian et al., 2014; Zhang et al., 2018; Peellage et al., 2022), frequencies in the range of 1–12 Hz have been utilised for subgrades of heavy haul or rather high-speed train lines. Therefore, a loading frequency of 8 Hz was used for the experiments in this study.

3. Results and discussion

3.1. Static stress-strain response

The conventional triaxial compression tests were performed under different confining pressures to obtain the peak deviatoric stresses and the corresponding shear strength values of the jointed rock samples under static loading. Fig. 4 shows the static deviatoric stress versus axial strain curves obtained from the static triaxial tests, and the corresponding peak deviatoric stress and shear strength values are reported in Table 2. The normal and shear stress

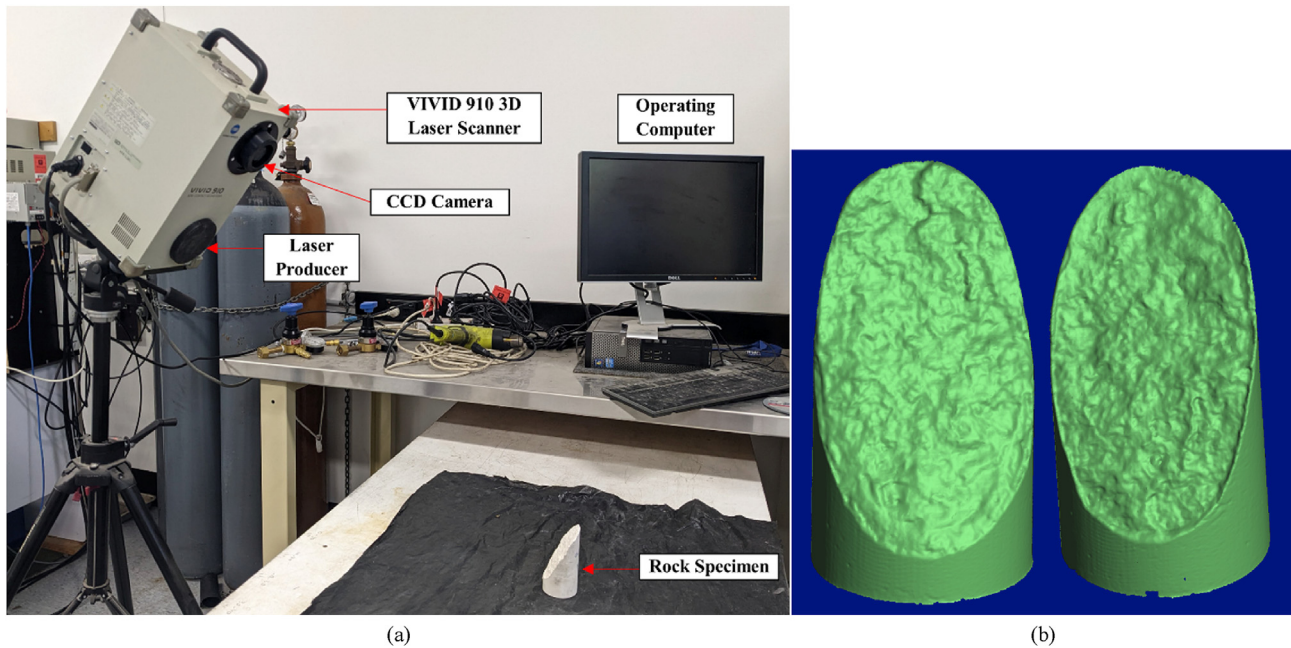


Fig. 3. (a) The non-contact 3D laser scanner (MINOLTA VIVID 910), and (b) Scanned 3D opposite surfaces of the jointed rock specimen.

components along the joint surface were determined from the principal stresses and the inclination angle of the joint as per the stress state on the joint surface as shown in Fig. 5 and using Eqs. (3a) and (3b).

$$\tau_s = \frac{(\sigma_1 - \sigma_3)\sin(2\theta)}{2} \quad (3a)$$

$$\sigma_n = \frac{\sigma_1 + \sigma_3}{2} + \frac{(\sigma_1 - \sigma_3)\cos(2\theta)}{2} \quad (3b)$$

where σ_1 is the major principal stress, σ_3 is the minor principal stress, τ_s is the shear stress on the joint plane, σ_n is the normal stress on the joint plane, and θ is the joint inclination angle.

The stress-strain plots in Fig. 4 indicate stick-slip behaviour possibly due to local sliding, over-riding and degradation of asperities accompanied by relocking of the broken and/or unbroken asperities during shearing (Byerlee, 1970). As shown in Fig. 4, with increased confining pressure, the jointed rock samples showed an increase in peak deviatoric stress as expected, and the axial strain required to achieve peak deviatoric stress was higher at low confining pressures (i.e. 15 kPa, 20 kPa and 25 kPa) than corresponding values at higher confining pressures (i.e. 90 kPa, 120 kPa and 150 kPa). The peak deviatoric stress and confining stress are used in Mohr-Coulomb analysis to obtain the corresponding shear strength, and the friction angle of the joint was determined to be 51° and comparable results were reported by other researchers (e.g. Premadasa 2013).

3.2. Cyclic stress-strain response

Figs. 6–8 present samples of cyclic stress-strain curves of the jointed rock samples, which are under the confining pressures of 20 kPa, 90 kPa and 150 kPa, respectively. According to Figs. 6–8, the stress-strain curve in the loading-unloading processes formed a hysteresis loop in each loading cycle. Under all the tested confining pressures, the hysteresis loops tended to change from sparse to dense with increasing number of cycles. This transition from sparse

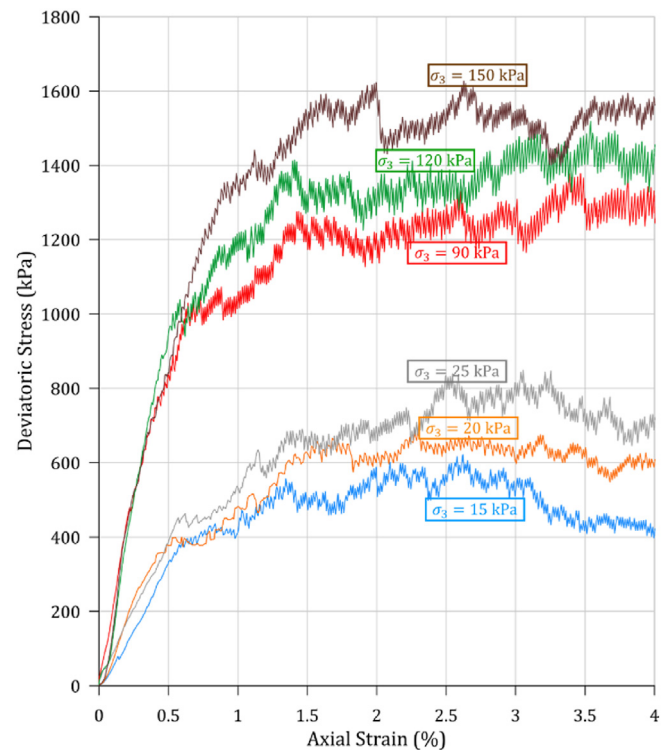


Fig. 4. The static stress-strain curves for jointed rock samples under confining pressures (σ_3) of 15 kPa, 20 kPa, 25 kPa, 90 kPa, 120 kPa and 150 kPa.

to dense hysteresis loops were more evident at lower confining pressures such as 20 kPa (Fig. 6) and higher cyclic deviatoric stress amplitudes (Figs. 7c and 8c).

Referring to the results, it is evident that the axial strain in each hysteresis loop consists of two portions, i.e. the elastic axial strain and plastic axial strain (residual axial strain). The elastic portion of the axial strain is recovered during the unloading process, while the

Table 2
Test conditions and results of jointed rock samples at static and dynamic failure.

Confining pressure, σ_3 (kPa)	Static peak deviator stress, q_{sp} (kPa)	Static shear strength, τ_s (kPa)	Critical dynamic stress, q_c (kPa)	Critical dynamic shear strength, τ_{cs} (kPa)	Ratio between q_c and q_{sp}	Ultimate residual axial strain (%)
15	601	260	400	173	0.66	9.48
20	687	298	450	195	0.65	8.96
25	801	347	500	217	0.62	8.39
90	1276	553	900	390	0.7	5.29
120	1439	623	1000	433	0.69	4.76
150	1627	705	1100	476	0.67	4.04

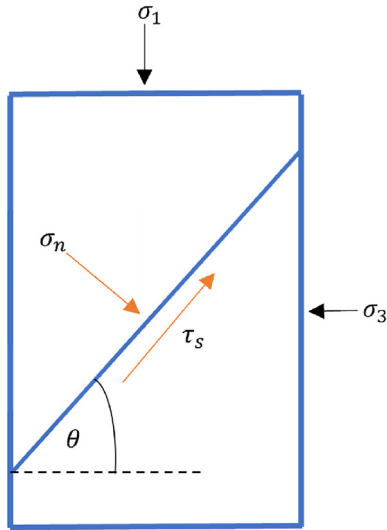


Fig. 5. Schematic diagram of the stress state at the joint surface.

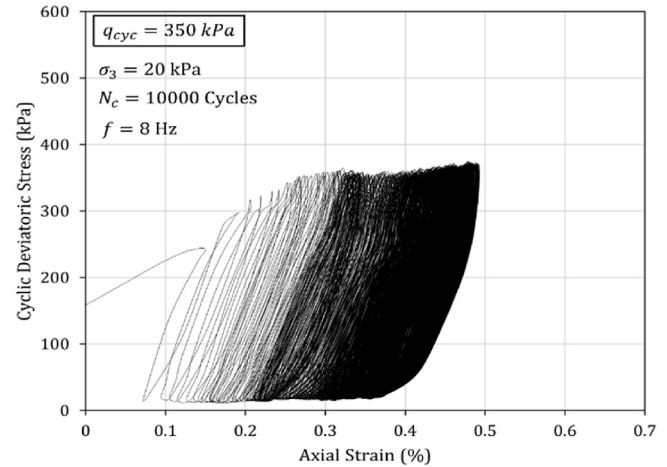
plastic portion is irreversible. The elastic axial strain ($\epsilon_{1,e}$), residual axial strain ($\epsilon_{1,p}$) and hysteresis loop in a loading cycle are illustrated in Fig. 9.

Fig. 10 shows samples of the hysteresis loops formed at different test conditions and different numbers of cycles and demonstrates the evolution of hysteresis loops under different loading conditions. Referring to Figs. 6–8 and 10, during the lower cyclic deviatoric stress amplitudes (i.e. $q_{cyc} < q_c$), the hysteresis loops nearly overlapped, and the loops were almost closed with a small residual axial strain, and only slight variations in the shape and area of the loops were observed. However, as the cyclic deviatoric stress amplitude exceeded the critical dynamic deviatoric stress (i.e. $q_{cyc} \geq q_c$) as evident in Figs. 6c, 7c and 8c, significant changes in the hysteresis loops accompanied by an increase in the height, breadth and the area of the loops were observed. During the initial loading cycles, the loops hardly overlapped, and the loading-unloading curves were no longer closed, indicating significant accumulation of plastic strains and energy dissipation. However, during the later stages of loading cycles, the loops gradually overlapped, and closed loops were formed with the indication of no further notable accumulation of residual axial strain until the end of the test. This observation is also evident from Figs. 6–8 and 10, where the accumulated residual axial strain increased with number of loading cycles and then stabilised.

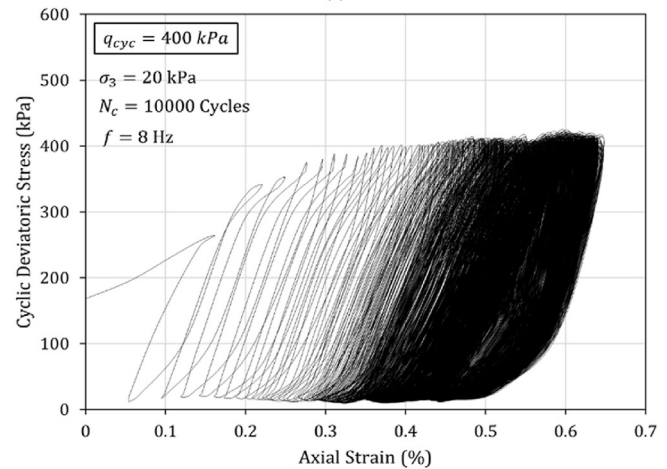
It should be noted that the amplitude of residual axial strain increment in each cycle became progressively lower. Accordingly, during the initial portion of the cyclic loading, the jointed rock samples exhibited viscoelastic plastic behaviour with increasing

irreversible axial strains, which is also reflected in the sparse hysteresis loops, while during the subsequent loading cycles, nearly viscoelastic behaviour was illustrated.

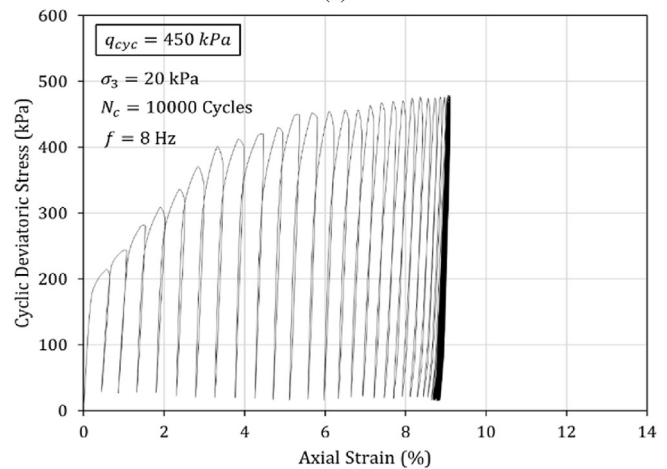
Moreover, a numerical analysis was conducted using the finite element software PLAXIS 3D to compare the experimental results



(a)



(b)



(c)

Fig. 6. The cyclic stress-strain curves for jointed rock samples under confining pressure (σ_3) of 20 kPa and cyclic deviatoric stress amplitudes (q_{cyc}) of (a) 350 kPa, (b) 400 kPa, and (c) 450 kPa.

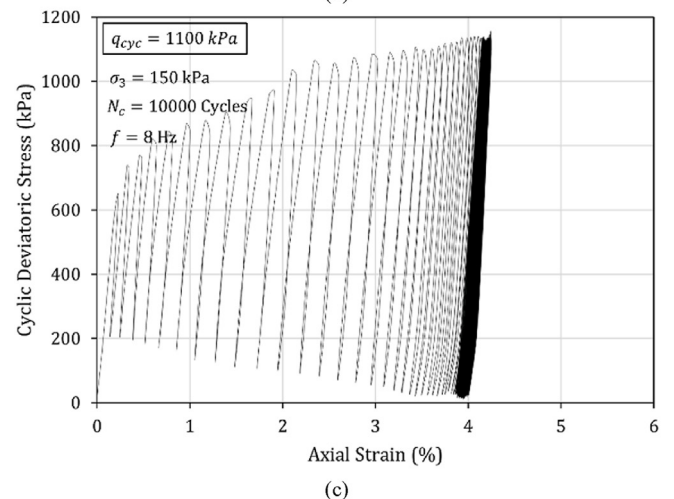
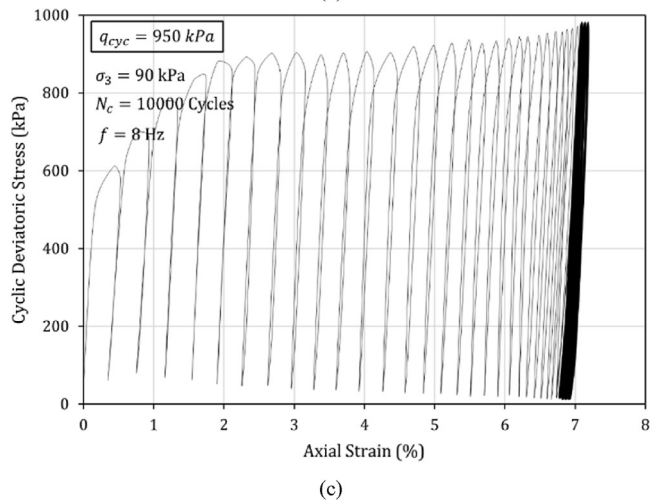
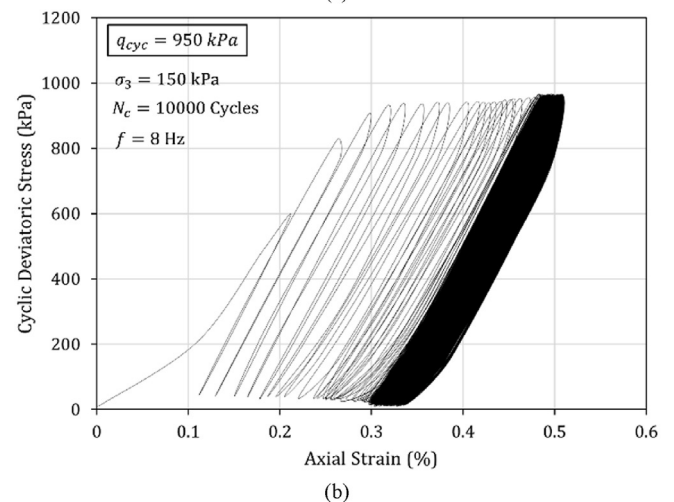
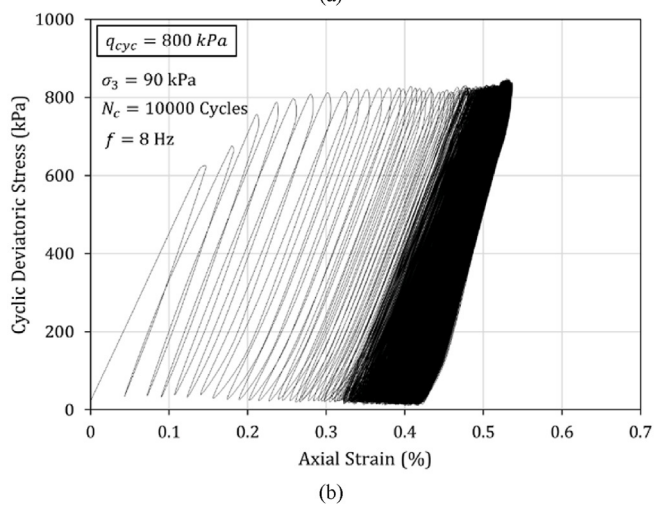
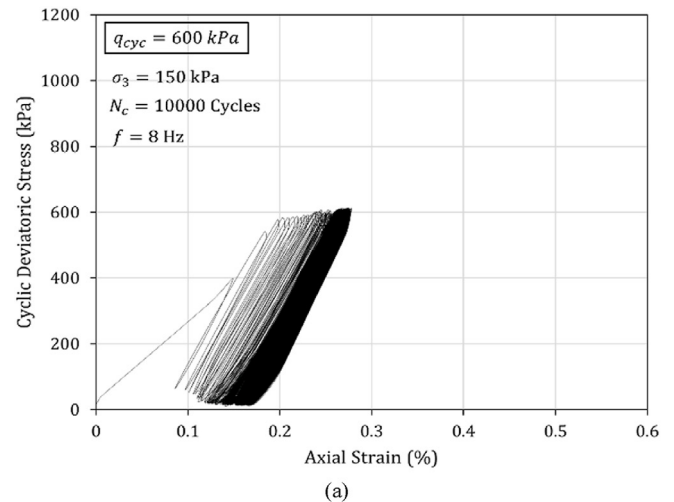
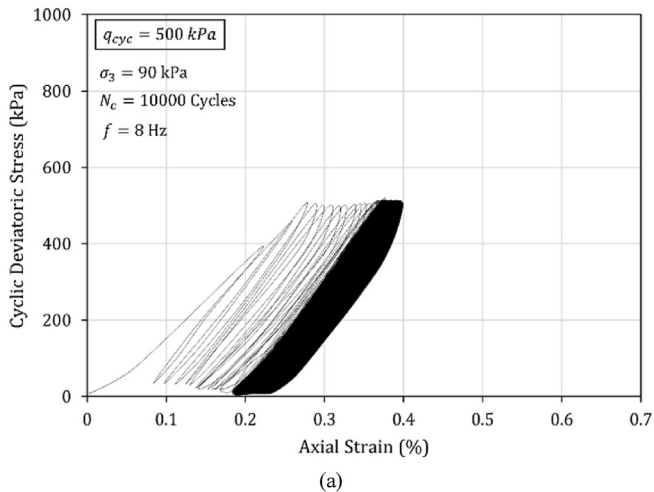


Fig. 7. The cyclic stress-strain curves for jointed rock samples under confining pressure (σ_3) of 90 kPa and cyclic deviatoric stress amplitudes (q_{cyc}) of (a) 500 kPa, (b) 800 kPa, and (c) 950 kPa.

Fig. 8. The cyclic stress-strain curves for jointed rock samples under confining pressure (σ_3) of 150 kPa and cyclic deviatoric stress amplitudes (q_{cyc}) of (a) 600 kPa, (b) 950 kPa, and (c) 1100 kPa.

with the numerical predictions. A 3D model of the jointed rock specimen with a diameter of 50 mm and height of 100 mm was created. The JR (jointed rock) model, which is available in PLAXIS 3D software capturing the joint direction and plasticity, was used as the constitutive model (PLAXIS, 2022). Shear strength parameters obtained from the stress-strain plots were used for the numerical

analysis, while a unit weight of 24 kN/m^3 and a Poisson's ratio of 0.2 were adopted. Young's modulus in the range of 80–120 MPa was used in the numerical analysis. It should be noted that since continuum-based modelling was used in this study, the elastic response of the jointed rock is governed by the elastic properties of the joint used in this study, which is more deformable than the

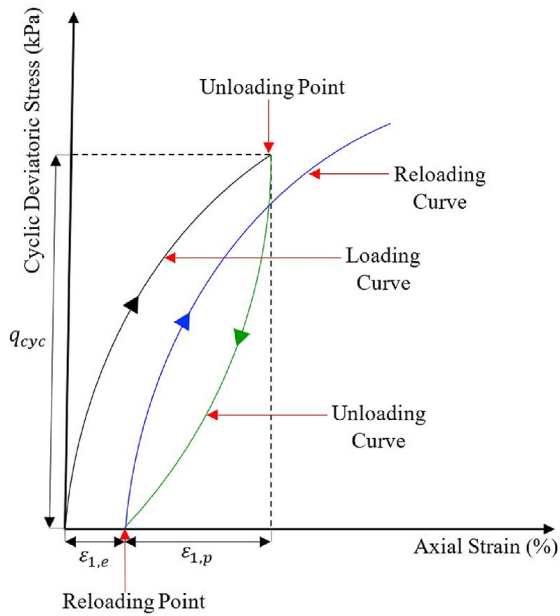


Fig. 9. Schematic diagram of a typical hysteresis loop in a loading cycle showing elastic axial strain ($\epsilon_{1,e}$) and residual axial strain ($\epsilon_{1,p}$) (after Zhang et al., 2017).

intact rock due to absence of cementation in the joint and reduced stiffness. With respect to displacement boundary conditions, the bottom boundary was fixed in the normal direction, while the side and top boundaries were kept free to simulate the cylindrical triaxial test. Dynamic analysis was conducted, allowing the application of cyclic loading with a cyclic deviatoric stress amplitude (q_{cyc}) of 400 kPa, and a confining pressure (σ_3) of 20 kPa. Fig. 11 shows the overview of the 3D finite element model and its characteristics.

Fig. 12 presents the comparisons of the dynamic stress-strain response of the rock in numerical modelling and experimental results for the first loading cycle. As evident in Fig. 12, the numerical predictions show when the sample was loaded to a certain stress level, the unloading curve was below the original loading curve, forming plastic hysteresis cycles, as also observed in the experimental results. Moreover, in both numerical and experimental results, the axial strain produced during the loading process did not recover completely during the unloading process, resulting in a residual axial strain at the end of the cycle.

3.3. Critical dynamic deviatoric stress

The critical dynamic deviatoric stress (q_c) reported here is the cyclic deviatoric stress amplitude at which the yielding of the jointed rock samples initiated under cyclic loading. Fig. 13 presents

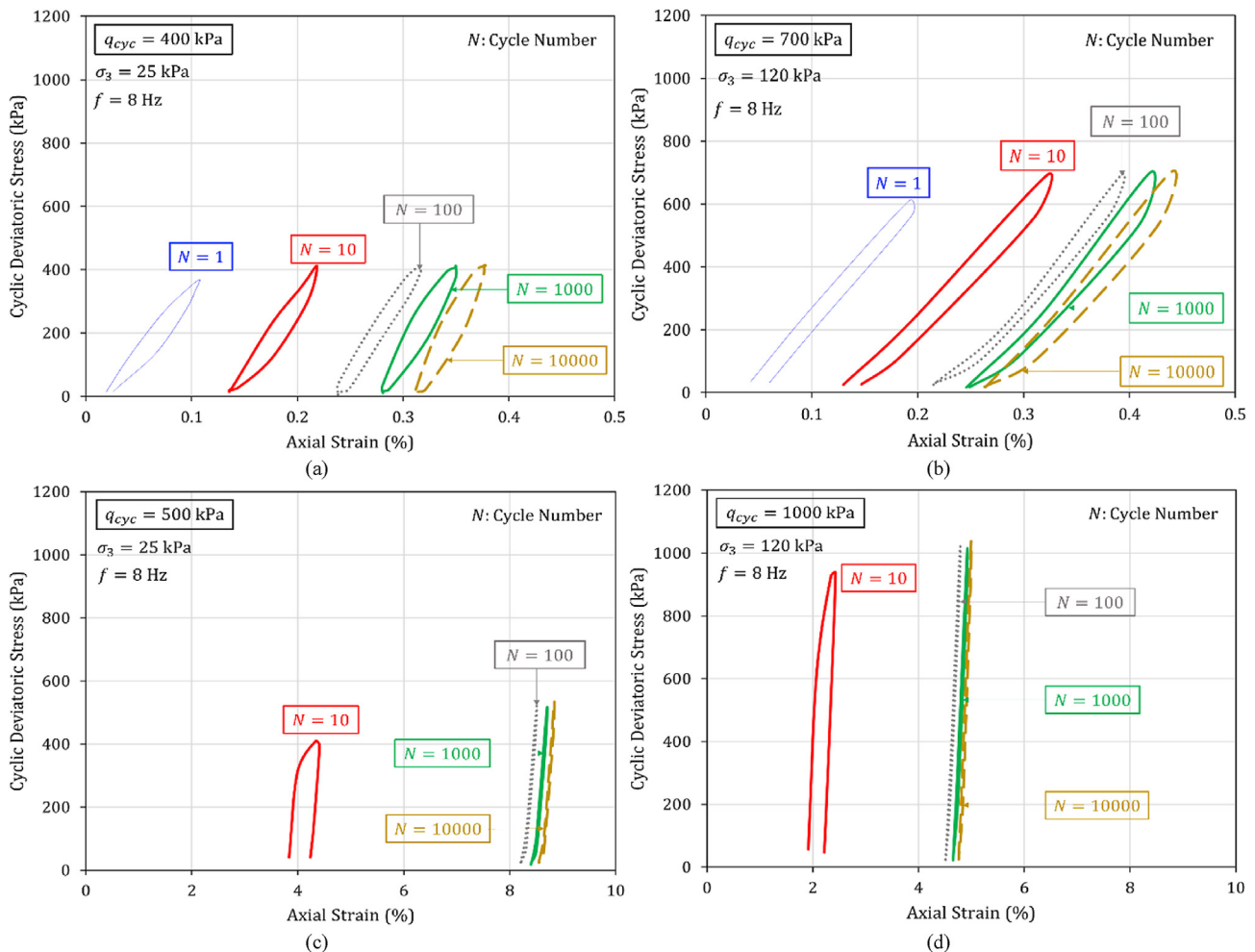


Fig. 10. Stress-strain hysteresis loops at various number of cycles at confining pressures (σ_3) and cyclic deviatoric stress amplitudes (q_{cyc}) of (a) $\sigma_3 = 25$ kPa and $q_{cyc} = 400$ kPa; (b) $\sigma_3 = 120$ kPa and $q_{cyc} = 700$ kPa; (c) $\sigma_3 = 25$ kPa and $q_{cyc} = 500$ kPa; and (d) $\sigma_3 = 120$ kPa and $q_{cyc} = 1000$ kPa.

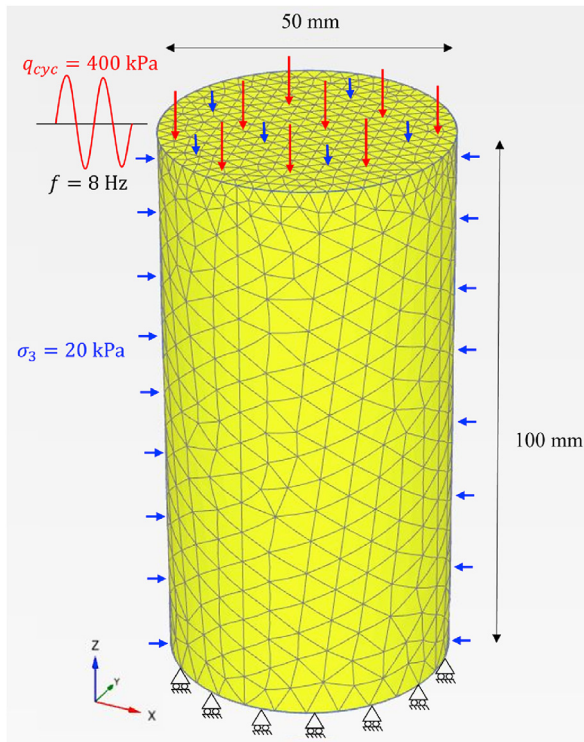


Fig. 11. Overview of the 3D finite element model.

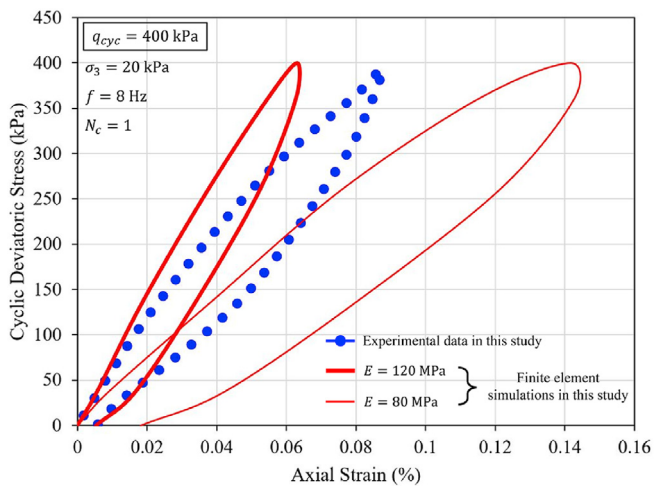


Fig. 12. Comparison of numerical predictions and laboratory measurements of cyclic stress-strain relationship for $q_{cyc} = 400$ kPa and $\sigma_3 = 20$ kPa.

how critical dynamic deviatoric stress and the corresponding peak deviatoric stress under static loading (q_s) varied with confining pressure. Table 2 reports the critical dynamic deviatoric stress values and the corresponding critical dynamic shear strength value calculated along the joint plane using Eqs. (3a) and (3b). As shown in Table 2 and Fig. 13, the critical dynamic deviatoric stress was always below the corresponding peak static deviatoric stress. According to Xiao et al. (2009), Momeni et al. (2015) and Jia et al. (2018), cyclic loading often causes rock masses to fail prematurely, i.e. at stress levels lower than the peak strength determined under static loading conditions. According to Table 2, the ratio between critical dynamic deviatoric stress and the corresponding peak deviatoric stress under static loading was in the range of 0.6–

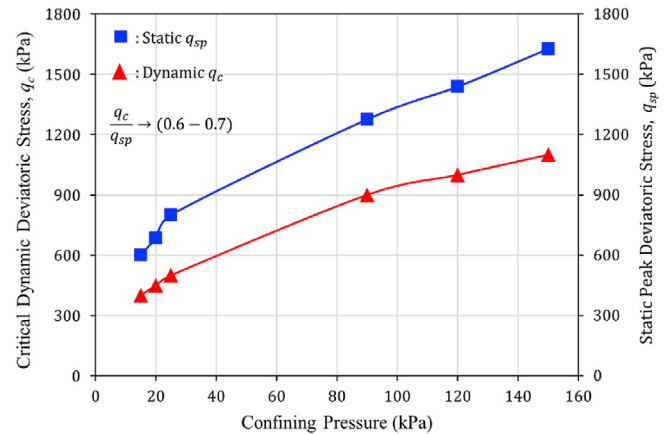


Fig. 13. Variations of critical dynamic stress and peak deviatoric stress under static loading with confining pressure.

0.7. It should be noted that the failure of intact rock samples under reduced dynamic stresses with the reduction factor in the range of 0.7–0.9 to be applied to static parameters was reported in the past by Bieniawski (1967) and Ma et al. (2013). Moreover, as evident in Fig. 13, the determined critical dynamic deviatoric stresses showed an increasing trend with the confining pressure. This behaviour could be due to the slower damage evolution of the jointed rock samples under higher confining pressures.

The critical number of cycles (N_c), defined as the cycle number at which the maximum residual axial strain per cycle would occur, were obtained from the results of cyclic triaxial tests with stress levels in excess of the critical dynamic deviatoric stress amplitude. The variation of critical number of cycles with cyclic stress ratio (CSR) (i.e. the ratio between cyclic deviatoric stress amplitude and two times applied confining pressure) is presented in Fig. 14. It is evident that the critical number of cycles was in the range of $N_c = 10$ –20. Yet, with increasing CSR, the critical number of cycles showed a slight reduction. This behaviour could be due to rapid damage evolution of the jointed rock samples under higher applied cyclic deviatoric stress or lower confining pressure, leading to a higher CSR.

3.4. Residual axial strain and damage evolution

Residual axial strain is defined as the axial strain at which the axial dynamic stress reaches the minimal value (Liu and He, 2012). In fact, when the axial dynamic stress reduces to the minimal value after a loading-unloading cycle, a portion of the axial strain will be recovered, and the remaining irreversible portion of the axial strain is the residual axial strain.

Fig. 15 illustrates how cumulative residual axial strain varied with number of cycles with increasing cyclic deviatoric stress amplitudes and subjected to different confining pressures (i.e. 15 kPa, 25 kPa, 90 kPa and 120 kPa). According to Fig. 15, at lower cyclic deviatoric stress amplitudes (i.e. $q_{cyc} < q_c$), as the number of cycles increased, the cumulative residual axial strain gradually increased and tended to stabilise. Indeed, in such conditions, the accumulated axial strains were minor, and they built up very slowly with the number of cycles, such that even if subjected to thousands of loading cycles, the growth of residual deformation was still so slow, showing no sign of yielding. Nevertheless, when the cyclic deviatoric stress amplitude exceeded the critical dynamic deviatoric stress (i.e. $q_{cyc} \geq q_c$), the residual axial strain rapidly increased during the initial loading cycles, and then gradually increased for a few more cycles and tended to stabilise until the end of cyclic

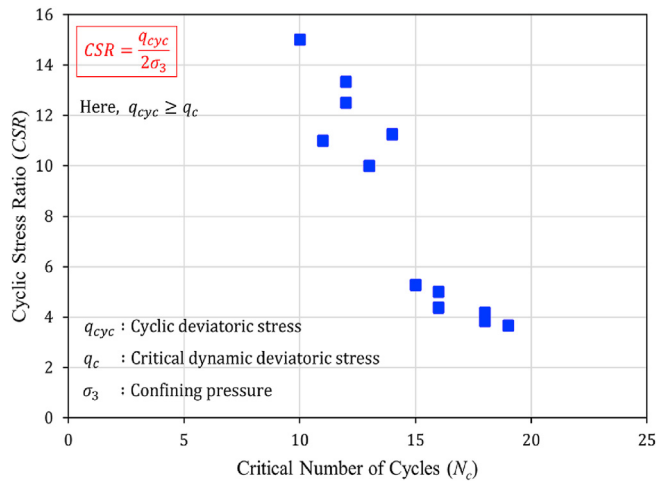


Fig. 14. Variation of critical number of cycles with cyclic stress ratio.

loading. Under such conditions, yielding of the joint was observed only after a few cycles, and the accumulated ultimate residual axial strains increased rapidly (Fig. 15).

Therefore, it can be concluded that this study shows a critical cyclic deviatoric stress amplitude (i.e. the critical dynamic deviatoric stress (q_c)) beyond which the yielding of the jointed rock specimens progressed remarkably, and comparable observations were also reported by Bagde and Petros (2005a) for intact sandstone specimens and Liu et al. (2021b) for jointed soft rock specimens.

The newly cast jointed rock specimens were scanned and digitised to obtain the initial JRC, which was measured to be $JRC_0 = 11.51$. After completion of the cyclic loading, the jointed rock specimens were dismantled from the apparatus and re-scanned and digitised again to obtain the final JRC (JRC_f) values as reported in Fig. 16. At lower cyclic deviatoric stress amplitudes (i.e. $q_{cyc} < q_c$), upon visual inspection of the joint after cyclic loading, damage to the asperities could not be seen in either halves of the joint with the naked eye, and thus a considerable difference between the initial and final JRC values was not expected. However, at the cyclic deviatoric stress amplitudes in excess of the critical dynamic deviatoric stress threshold (i.e. $q_{cyc} \geq q_c$), a considerable damage to the asperities of the jointed rock specimen could be observed visually. Fig. 17 presents samples of the damaged surfaces of the jointed rock specimens obtained at critical dynamic deviatoric stresses corresponding to the confining pressures of 25 kPa, 90 kPa and 150 kPa.

According to Brady and Brown (1993), the deformation of a natural jointed rock mass occurs as a result of combined asperity sliding and asperity damage. Asperity damage, in its mechanical sense, refers to a state at which micro-cracks are initiated and grown in rock masses under the effect of external loading, and the cracks may emerge as macro-fractures or macroscopically visible fractures (Martin and Chandler, 1994). Moreover, the deformation behaviour of a natural jointed rock mass depends mainly on the strength, size and shape of the asperities, inclination of the joint and the stresses applied on the jointed rock mass (Lee et al., 2001; Guo and Qi, 2015; Zhang et al., 2019). Therefore, under the effect of lower cyclic deviatoric stress amplitudes, micro-cracks would be formed on the asperities of the joint surface accompanied by slight sliding of the asperities, and these micro-cracks would barely amplify into macro-cracks. However, when stresses exceed the critical dynamic deviatoric stress, micro-cracks would form on the asperities, which would grow into macro-cracks triggering

macroscopic damage and excessive deformation of the jointed rock sample as also evident from Figs. 15 and 17.

According to Fig. 17, the damage to the jointed rock specimen was concentrated to certain areas of the surface, possibly with the highest asperities. With the application of the cyclic loading, the micro-cracks developed into macro-cracks, damaging the tips of the highest asperities of the joint surface, and during this deformation process, the degraded materials formed into gouge and accumulated on the valleys of the joint surface depending on the shear direction. According to Huang et al. (1993), this rubblised degraded material in the valleys of the joint surface usually becomes very firmly compacted and reattached to the joint surface, as also observed in the tested samples. Moreover, the surface of the rubblised asperity gouge and sheared off asperity heads was smooth, as in a planar joint surface.

Fig. 16 presents how the final JRC values under the critical dynamic deviatoric stresses varied with confining pressure. The ultimate residual axial strain (ϵ_{pu}) reported here is the cumulative residual axial strain attained by the jointed rock sample at the end of cyclic loading. Referring to Table 2 and Figs. 15–17, with increasing confining pressure, the critical dynamic deviatoric stress increased, the corresponding ultimate residual axial strain decreased, and the damage to asperities of the joint surface increased, resulting in a decrease in the final JRC of the joint surface. Accordingly, under the effect of high confinement, deformation of the joint is restricted, and the cyclic deviatoric stress amplitude should be high enough to cause asperity damage and deformation of the joint. It should be noted that at such conditions, asperity damage will be dominated over asperity overriding.

3.5. Prediction of cumulative residual axial strain

Over the years, several empirical and analytical models have been proposed to predict the cyclic cumulative deformation behaviours of different geotechnical materials. Among them, the power equation proposed by Monismith et al. (1975) has been widely used with modifications to predict cumulative plastic deformation of different geomaterials. Referring to Fig. 15, under lower cyclic deviatoric stress amplitudes (i.e. when $q_{cyc} < q_c$), the ultimate residual axial strains developed in the jointed rock specimen were insignificant when compared to the ultimate residual axial strains developed under higher cyclic deviatoric stress amplitudes (i.e. when $q_{cyc} \geq q_c$). Moreover, referring to Fig. 15, the cumulative residual axial strain curves showed an increasing trend with increasing cyclic deviatoric stress amplitude and a decreasing trend with the increasing confining pressure. It should be noted that the critical dynamic deviatoric stress is a function of joint properties such as joint roughness, joint strength and joint inclination that would influence the residual axial strains developed in the jointed rock specimens. Therefore, number of cycles, applied cyclic deviatoric stress, confining pressure and critical dynamic deviatoric stress were considered as independent parameters required for formulating an empirical relationship to predict residual axial strain (ϵ_p), as in Eqs. (4a)–(4d), based on the experimental results reported in Fig. 15.

$$\epsilon_p = \begin{cases} \alpha (N^\beta) \tanh(\beta N) \left(\frac{R_q}{1 + 1/CSR} \right)^\lambda & (q_{cyc} \geq q_c) \\ 0 & (q_{cyc} < q_c) \end{cases} \quad (4a)$$

where

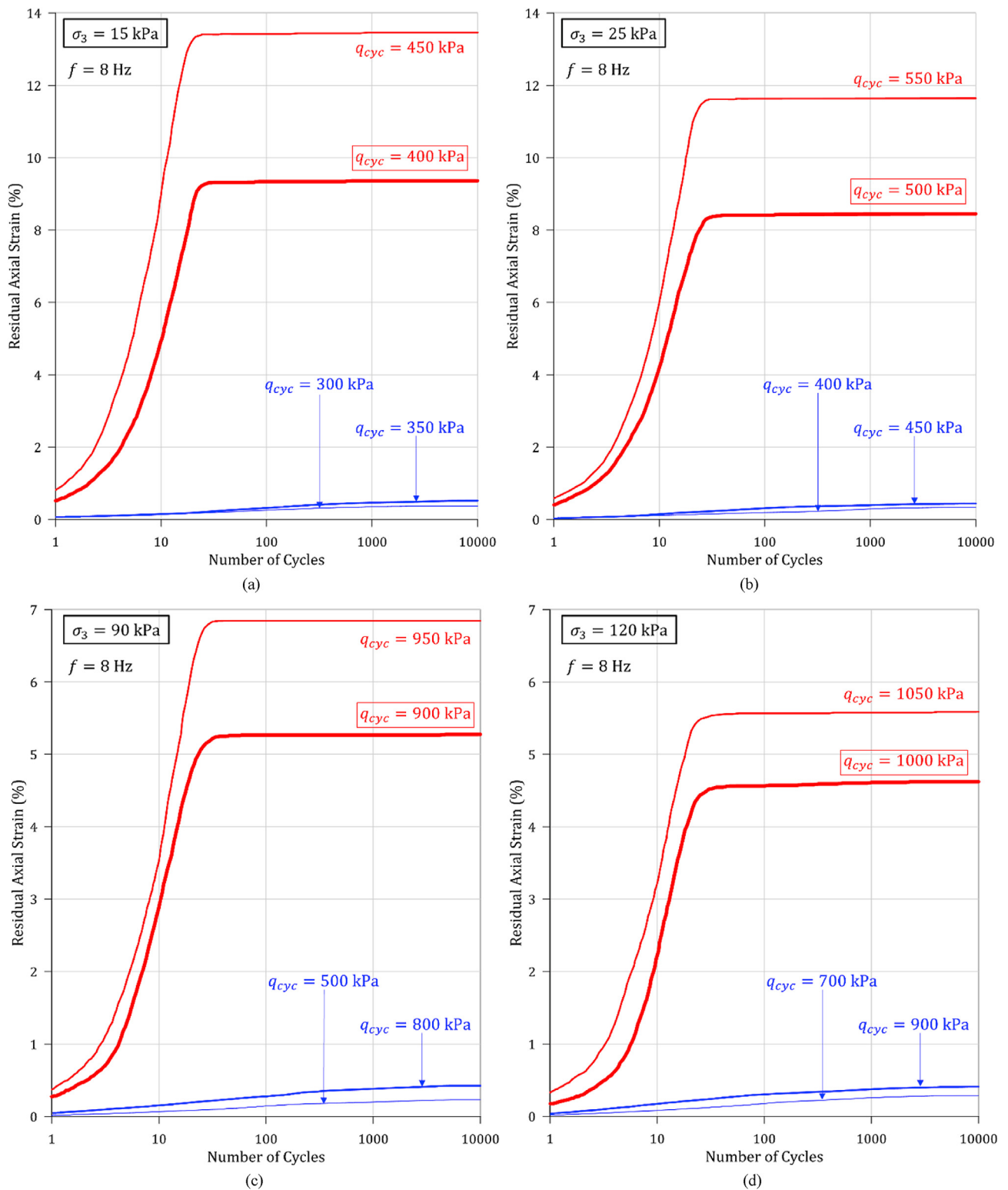


Fig. 15. The residual axial strain evolution curves under different cyclic deviatoric stress amplitudes (q_{cyc}) and confining pressures (σ_3) of (a) 15 kPa, (b) 25 kPa, (c) 90 kPa, and (d) 120 kPa.

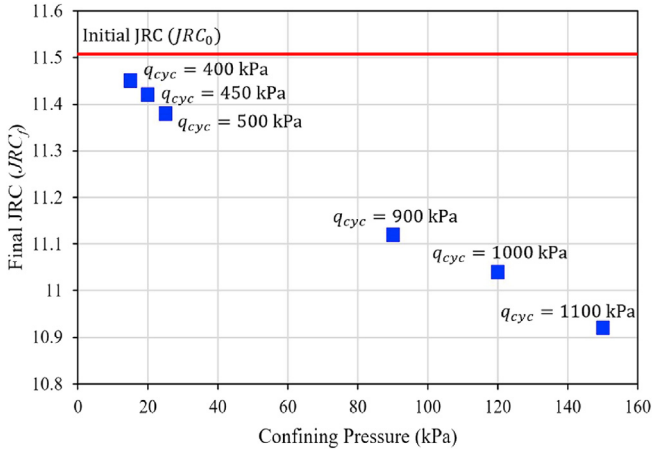


Fig. 16. Variation of final JRC values (JRC_f) of jointed rock samples subjected to critical dynamic stress (q_c) with confining pressure (σ_3).

$$R_q = \frac{q_{cyc}}{q_c} \tag{4b}$$

$$CSR = \frac{q_{cyc}}{2\sigma_3} \tag{4c}$$

$$q_c = Kq_{sp} \tag{4d}$$

where N is the number of cycles, R_q is the dynamic deviatoric stress ratio, σ_3 is the applied confining stress, and q_{sp} is the peak deviatoric stress under static triaxial loading condition. In this study, the critical dynamic deviatoric stress determined from the cyclic triaxial tests was correlated to the peak deviatoric stress under static loading via Eq. (4d), where K was determined to be 0.68. Additionally, α , β and λ are empirical constants obtained based on data fitting exercise, which depend on the joint characteristics such as joint roughness, joint inclination, and joint wall compressive strength. It should be noted that since the value of cyclic deviatoric stress amplitude for each loading cycle could slightly deviate from the target input value particularly when sample experiences large deformation, a weighted average of cyclic deviatoric stress amplitude was used for each test as recommended by ASTM D5311-13 (2013) and reported in Eq. (5).

$$(q_{cyc})_{avg} = \frac{1}{N_i} \sum_{n=1}^{N_i} (q_{cyc})_n \tag{5}$$

where $(q_{cyc})_{avg}$ is the average value of cyclic deviatoric stress amplitude, $(q_{cyc})_n$ is the cyclic deviatoric stress amplitude at a given cycle n , and N_i is the total number of cycles for a particular test.

In this study, the values of the empirical constants were obtained through a nonlinear regression analysis programmed in MATLAB using the nonlinear least squares method and trust-region algorithm as $\alpha = 7.843$, $\beta = 0.068$ and $\lambda = 5.488$. Fig. 18 presents the predicted residual axial strains from Eqs. (4a)-(4d) versus the laboratory measurements in the 3D space, while Fig. 19 illustrates the same in the 2D space for the confining pressures of 25 kPa and 90 kPa as examples.

3.6. Resilient modulus

As discussed in the previous sections, the axial deformation during cyclic loading can be divided into two categories; elastic

deformation which is recoverable in the unloading process, and plastic deformation, which is irreversible and accumulates with further cyclic loading. The resilient modulus (M_R) is a parameter capturing elastic deformation characteristics during the cyclic loading-unloading process. In fact, it specifically captures the unloading characteristics of the tested specimens related to the

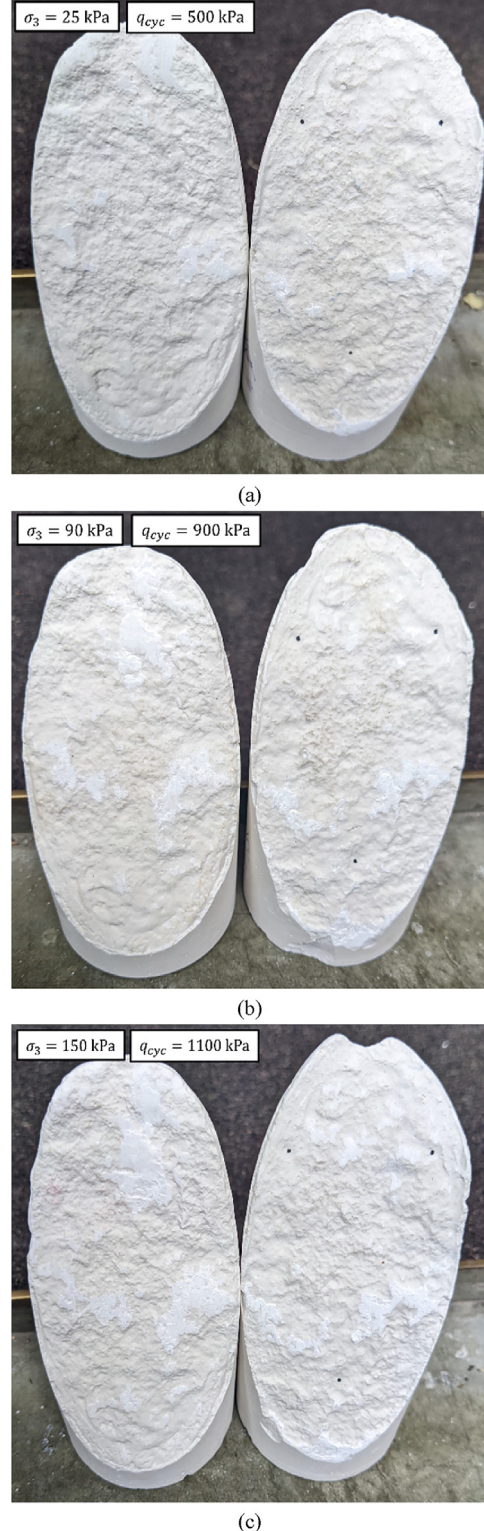


Fig. 17. Samples of damaged surfaces of the jointed rock specimens at peak deviatoric stress amplitude at confining pressures (σ_3) of (a) 25 kPa, (b) 90 kPa, and (c) 150 kPa.

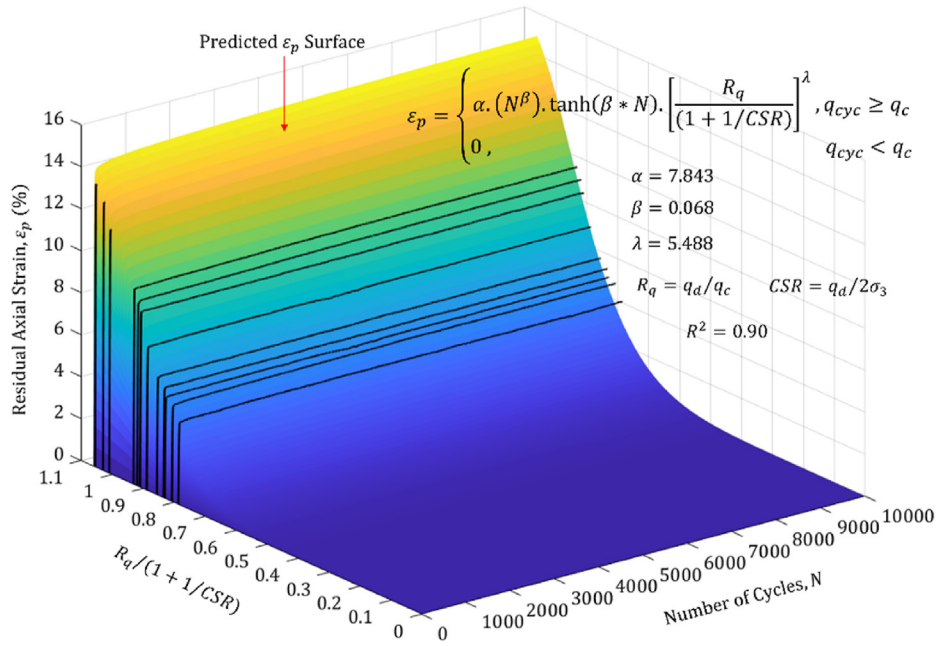


Fig. 18. Variation of actual and predicted residual axial strain (ϵ_p) in the 3D space.

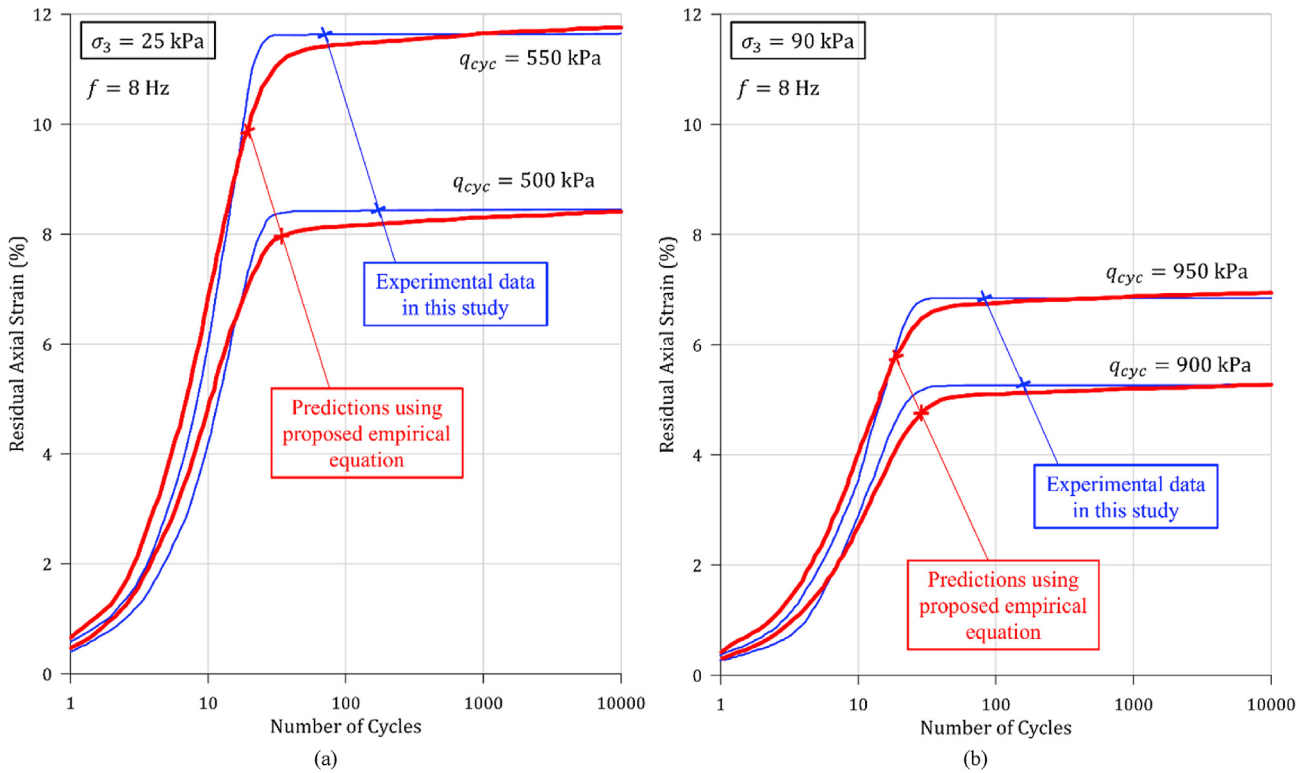


Fig. 19. The predicted and experimentally obtained residual axial strain evolution curves under cyclic deviatoric stress amplitudes (q_{cyc}) exceeding the critical dynamic stress and confining pressures (σ_3) of (a) 25 kPa and (b) 90 kPa.

reversible axial strains recovered during the unloading process, and is defined as follows:

$$M_R = \frac{\Delta q_{cyc}}{\epsilon_{1,e}} \quad (6)$$

where Δq_{cyc} is the difference between the maximum and minimum cyclic deviatoric stresses, i.e. from the beginning point of unloading to the beginning point of reloading; and $\epsilon_{1,e}$ is the recoverable axial strain during unloading as schematically shown in Fig. 9. Fig. 20 presents the variation of resilient moduli with number of loading cycles with increasing cyclic deviatoric stress amplitudes for the

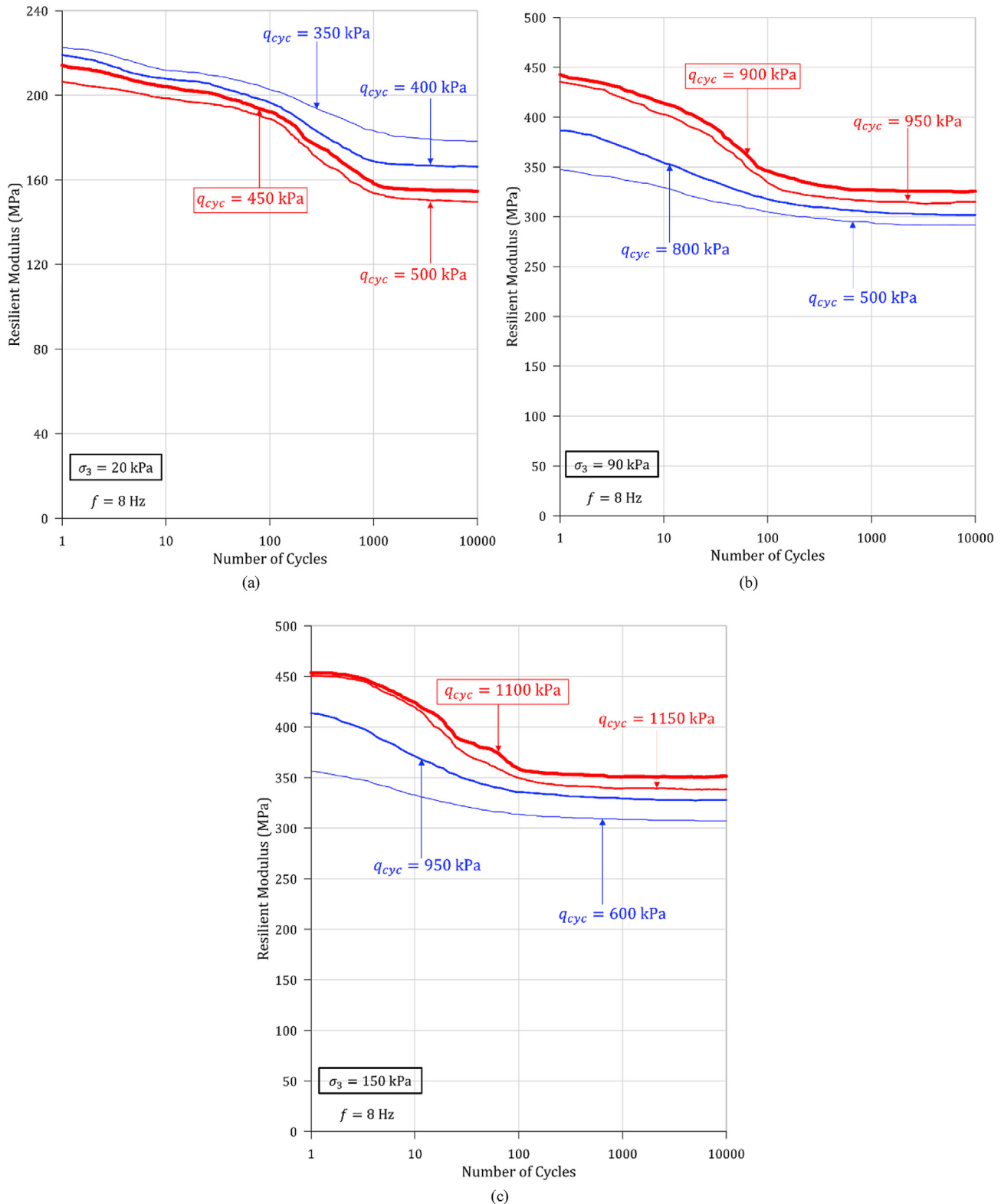


Fig. 20. The resilient modulus evolution curves under different cyclic deviatoric stress amplitudes (q_{cyc}) and confining pressures (σ_3) of (a) 20 kPa, (b) 90 kPa, and (c) 150 kPa.

confining pressures of 20 kPa, 90 kPa and 150 kPa for the jointed rock used in this study. According to Fig. 20, at lower cyclic deviatoric stress amplitudes (i.e. when $q_{cyc} < q_c$), the resilient moduli gradually degraded with number of cycles and tended to stabilise at

later stages. It is evident that for the cyclic deviatoric stress amplitudes in excess of critical dynamic deviatoric stress (q_c), the degradation of the resilient moduli with number of cycles was quite rapid during the initial loading cycles, then gradually slowed down

and stabilised during the later loading cycles. Comparable trends for the evolution of resilient moduli with the number of loading cycles were also reported by Fuenkajorn and Phueakphum (2010), Ma et al. (2013) and Wang et al. (2013) for intact rock samples and Liu et al. (2018b) and Zheng et al. (2020a) for jointed rock samples.

Referring to Fig. 20, at cyclic deviatoric stress amplitudes less than the critical dynamic deviatoric stress, the slight degradation of resilient moduli during the initial loading cycles and the subsequent stabilisation during the rest of the loading cycles could be due to the formation of micro-fractures and slight sliding of asperities, which did not amplify into macroscopic deformation and insignificant damage of the joint. When cyclic deviatoric stress amplitude exceeded the critical dynamic deviatoric stress, the substantial degradation of the resilient moduli could be due to amplification of micro-cracks into macro-fractures accompanied by asperity sliding forming notable damage to the joint surface. Moreover, Fig. 20 illustrates that the deterioration of the resilient moduli increased with cyclic deviatoric stress amplitude and reduced with the confining pressure. Slower deterioration of the resilient moduli with increased confining pressure could be due to slower damage evolution and sliding of the asperities of the jointed rock specimen under higher confining pressures as also reported by Liu et al. (2011).

4. Dynamic energy evolution and damping response

The deformation and failure mechanism of rock masses can be explained from the perspective of energy evolution based on energy theories and principles. According to Song et al. (2020), under laboratory conditions, the energy evolution of a rock specimen under external loading can be categorised into four processes, i.e. energy input, energy accumulation, energy dissipation and energy release. Under triaxial loading conditions, the loading actuator applies an axial load on the jointed rock specimen, which is energy input to the jointed rock specimen. Without considering other energy losses, a portion of this input energy will be accumulated in the form of elastic deformation energy which will cause the elastic deformation of the jointed rock specimen and will be released when unloading. The other portion of the energy will be dissipated leaving plastic deformation in the jointed rock specimen. The relationship among external energy input (ΔE), elastic energy stored in the rock (ΔE_e) and dissipated energy by the rock in the loading-unloading process (ΔE_d) is given by the following expression:

$$\Delta E = \Delta E_e + \Delta E_d \quad (7)$$

In the cyclic triaxial tests, these types of energy can be determined from the cyclic stress-strain response of the jointed rock specimen as reported in Figs. 6–8. A schematic diagram of a loading-unloading cycle at a given stress level representing these types of energy is shown in Fig. 21. According to Fig. 21a, the area under the loading curve represents the energy absorbed by the jointed rock specimen (i.e. input energy) for a given cycle, which represents the total work done by the actuator of the cyclic triaxial apparatus. The area under the unloading curve represents the elastic energy stored by the jointed rock specimen, which is also released during the unloading. As shown in the cyclic stress-strain curves in Figs. 6–8, for a given cycle, after loading to a certain stress level, the unloading curve does not coincide with the loading curve, forming a hysteresis loop. Referring to Fig. 21a, the area of the hysteresis loop captures the energy dissipated from the jointed rock specimen in a given cycle. More precisely, the area of the hysteresis loops in the cyclic stress-strain curves gives the dissipated energy density and when it is multiplied by the sample volume, the dissipated energy during loading-unloading cycles can be determined. In this study, a MATLAB code was developed to calculate the area within the hysteresis loop in each cycle adopting data collected from the cyclic triaxial tests.

Fig. 22 presents how the dissipated energy density per load cycle varied with number of loading cycles. As evident in Fig. 22, at lower cyclic deviatoric stress amplitudes (i.e. when $q_{cyc} < q_c$), the dissipated energy density slightly increased and decreased promptly during the initial loading cycles and reached a steady state gradually. Referring to Fig. 22, when the cyclic deviatoric stress amplitude exceeded the critical dynamic deviatoric stress (i.e. when $q_{cyc} \geq q_c$), the dissipated energy density drastically increased to an exorbitant value and decreased dramatically during the initial loading cycles and then stabilised gradually. Comparable trends for the evolution of dissipated energy with the number of loading cycles when $q_{cyc} < q_c$ were also reported by Momeni et al. (2015) and Yang et al. (2018) for intact rock specimens and Liu et al. (2017, 2018) for intermittently jointed rock samples. When $q_{cyc} \geq q_c$, comparable trends were also reported by Zhang et al. (2017) for intact red sandstone specimens.

Fig. 23 illustrates how initial dissipated energy density per load cycle and steady state dissipated energy density per load cycle values varied with applied cyclic deviatoric stress amplitudes for the confining pressures of 20 kPa and 120 kPa. The initial dissipated per load cycle (ΔE_{di}) and steady-state dissipated energy per

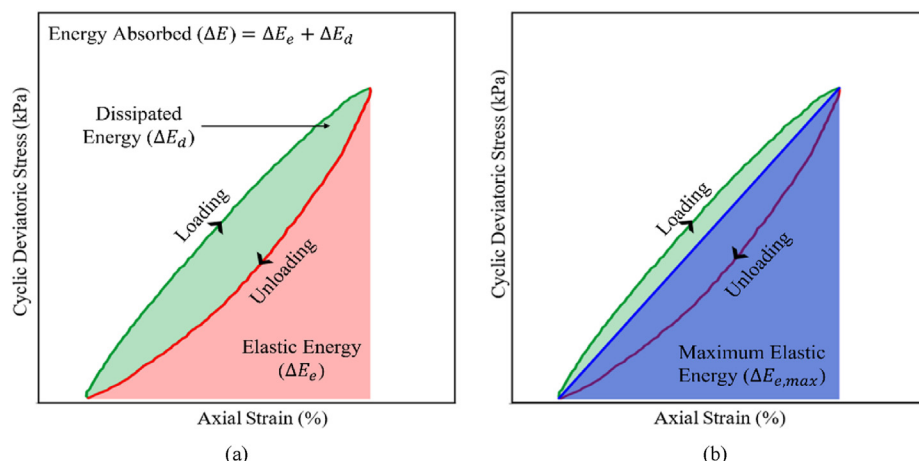


Fig. 21. Schematic diagrams of a typical hysteresis loop showing (a) dissipated energy, elastic energy and energy absorbed; and (b) maximum elastic energy.

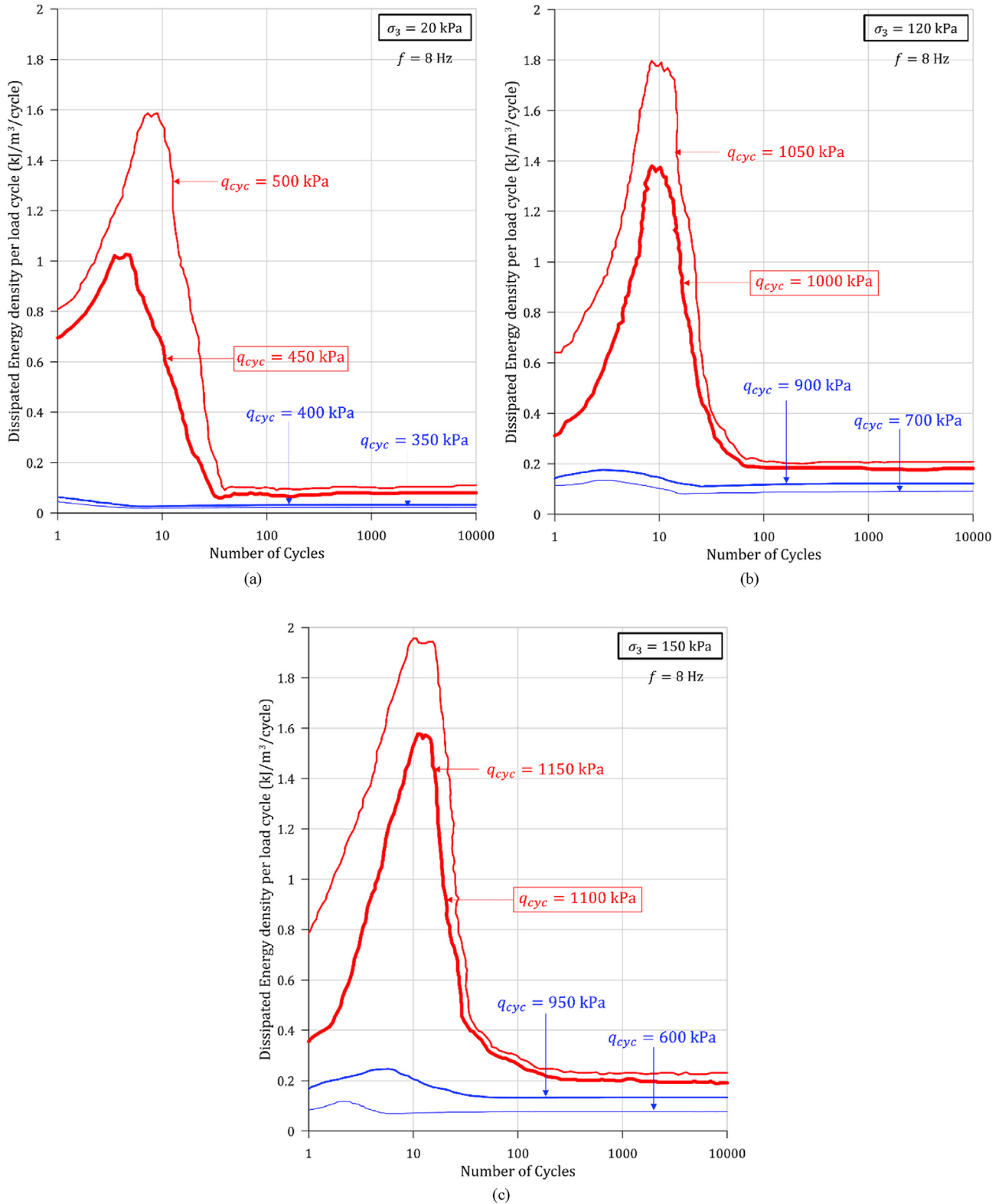


Fig. 22. The evolution of dissipated energy at different cyclic deviatoric stress amplitudes (q_{cyc}) and under confining pressures (σ_3) of (a) 20 kPa, (b) 120 kPa, and (c) 150 kPa.

load cycle (ΔE_{dc}) reported here are the calculated values of dissipated energy densities of the first loading cycle and final loading cycle, respectively. Here, the weighted average values of cyclic deviatoric stress amplitudes, calculated using Eq. (5) were used to

plot results in Fig. 23. Referring to Figs. 22 and 23, both initial dissipated energy per load cycle and steady-state dissipated energy per load cycle increased with cyclic deviatoric stress amplitude. Yet, the initial dissipated energy per load cycle values when the cyclic

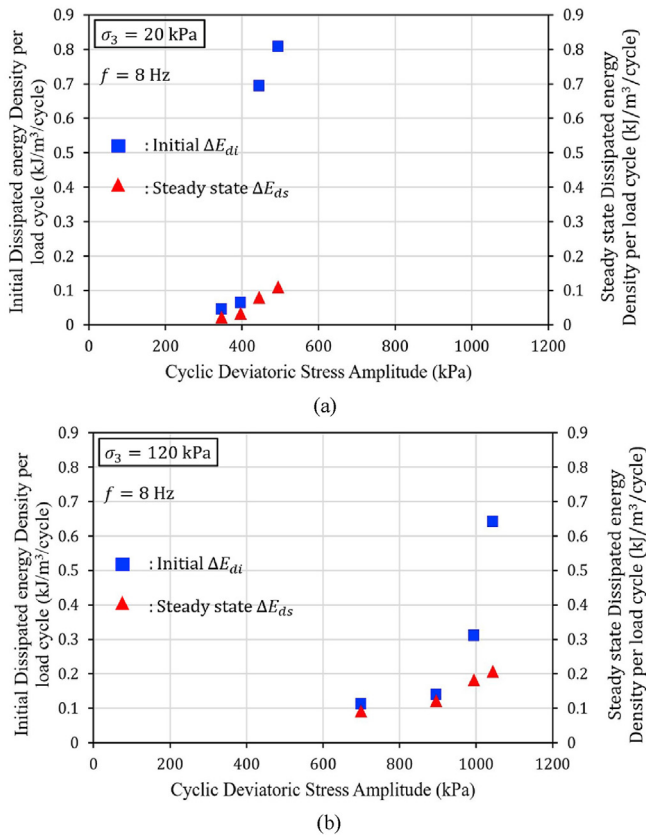


Fig. 23. Variation of initial dissipated energy density and steady-state dissipated energy density per load cycle with cyclic deviatoric stress amplitude (q_{cyc}) at confining pressures (σ_3) of (a) 20 kPa and (b) 120 kPa.

deviatoric stress amplitude exceeded the critical dynamic deviatoric stress threshold (i.e. $q_{cyc} \geq q_c$) were significantly higher than the corresponding values at lower cyclic deviatoric stress amplitudes (i.e. $q_{cyc} < q_c$).

As stated by Zhang et al. (2017), Song et al. (2020) and He et al. (2021), the dissipated energy reflects work done on crack initiation, propagation and coalescence in a rock mass under loading-unloading conditions, i.e. dissipated energy causes the irreversible material deterioration and plastic deformation of the jointed rock samples. Accordingly, at lower cyclic deviatoric stress amplitudes, a considerably large portion of input energy is dissipated (as also explained by Liu et al. (2017)) causing some irreversible deformation during the initial loading cycles. Since the dissipated energy under the applied cyclic deviatoric stress amplitude was not sufficient enough to amplify the micro-cracks into macro-cracks, dissipated energy density per load cycle progressively decreased and stabilised (Fig. 22), causing the irreversible deformation of the joint per load cycle to progressively decrease and stabilise (Fig. 15).

When applied cyclic deviatoric stress amplitude exceeded the critical dynamic deviatoric stress, a huge portion of the input energy was dissipated, which increased promptly during the initial loading cycles (Fig. 22). This dissipation of energy caused amplification of the micro-cracks into macro-cracks accompanied with major asperity sliding, resulting in extensive irreversible degradation and deformation of the joint (Fig. 15). Since the application of the cyclic load was continued even after joint reached the ultimate residual deformation, the dissipated energy per load cycle

promptly decreased and stabilised (Fig. 22) causing the accumulated residual deformation of the joint to reach a steady state (Fig. 15), i.e. the jointed rock specimens which deformed extensively during the initial loading cycles became stable again and recovered the ability to accumulate energy causing the dissipated energy to decrease promptly, as also reported by Zhang et al. (2017). However, due to the reduction of energy storage capacity of the jointed rock specimens caused by plastic deformation and damage, the proportion of dissipated energy could not return to its previous levels as shown in Fig. 23.

The damping ratio for a given hysteresis loop in cyclic triaxial testing can be determined as

$$\xi = \frac{\Delta E_D}{\pi \Delta E_{e,max}} \quad (8)$$

where ΔE_D is the inner area of the hysteresis loop indicating energy dissipated in one loading cycle (Fig. 21a), and $\Delta E_{e,max}$ is the maximum elastic energy stored on one loading cycle approximated by the area of the shaded triangle as shown in Fig. 21b.

Fig. 24 presents how the damping ratio per load cycle values evolved with number of cycles for different cyclic deviatoric stress amplitudes and confining pressures. As shown in Fig. 24, the damping ratio per load cycle decreased eminently during the initial loading cycles and then recovered slightly and stabilised eventually. The descent of the damping ratio per load cycle with increasing number of cycles was more abrupt when the cyclic deviatoric stress amplitude exceeded the critical dynamic deviatoric stress (Fig. 24). The initial damping ratio per load cycle (ξ_i) and steady-state damping ratio per load cycle (ξ_s) stated here are the calculated damping ratio values of the first loading cycle and final loading cycle, respectively. As evident from Fig. 24, the initial damping ratio per load cycle values increased when cyclic deviatoric stress amplitudes increased. Nevertheless, when cyclic deviatoric stress amplitude values surpassed the critical dynamic deviatoric stress, the calculated initial damping ratio per load cycle increased notably. Referring to Fig. 24, the values of initial damping ratio per load cycle were in the range of 40%–80% under higher cyclic deviatoric stress amplitudes (i.e. $q_{cyc} \geq q_c$), whereas under lower cyclic deviatoric stress amplitudes (i.e. $q_{cyc} < q_c$), the initial damping ratio per load cycle values were in the range of 5%–35%. Nevertheless, the steady-state damping ratio per load cycle values were below 12% under all the tested cyclic deviatoric stress amplitudes and confining pressures.

Accordingly, when lower cyclic deviatoric stress amplitudes were applied (i.e. $q_{cyc} < q_c$), a significant portion of the input energy was dissipated (Fig. 22) than being stored as elastic energy during the initial loading cycles, resulting in some residual deformation of the joint and considerably higher damping ratios. Since the applied load was not sufficient to cause macroscopic damage and residual deformation, damping ratio per load cycle decreased and reached a steady state. When the applied cyclic deviatoric stress amplitude exceeded the critical dynamic deviatoric stress (i.e. $q_{cyc} \geq q_c$), a significant portion of the input energy was dissipated (Fig. 22), allowing minimum amount of stored elastic energy, resulting in macroscopic deformation of the joint and extensive damping ratios during the initial loading cycles, as illustrated in Fig. 24. Under these higher cyclic deviatoric stress amplitudes (i.e. $q_{cyc} \geq q_c$), as the cyclic load continued, the accumulated residual axial deformation stabilised (Fig. 15) while the damping ratio per load cycle decreased and stabilised with further loading.

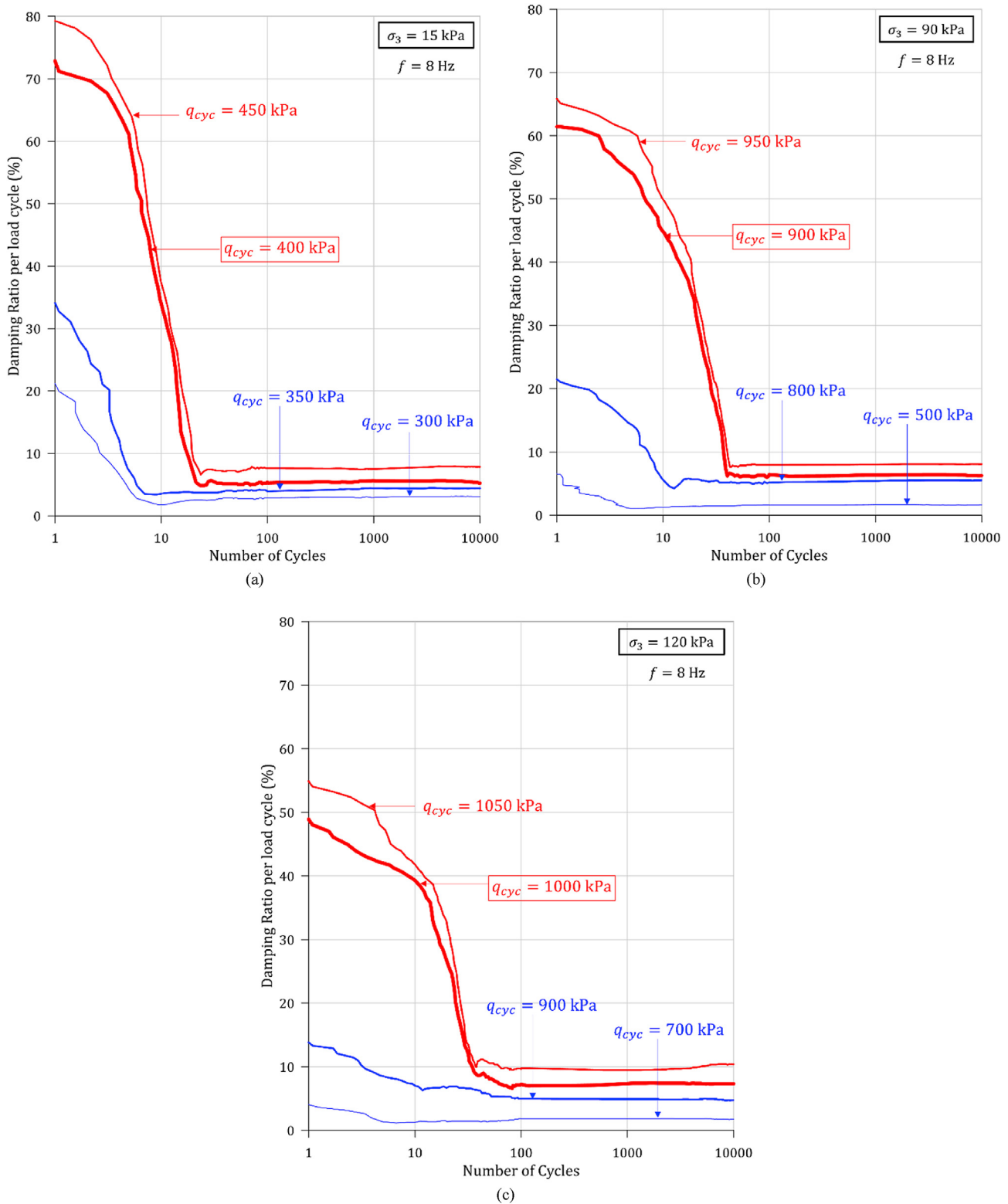


Fig. 24. The evolution of damping ratio at different cyclic deviatoric stress amplitudes (q_{cyc}) under confining pressures (σ_3) of (a) 15 kPa, (b) 90 kPa, and (c) 120 kPa.

5. Conclusions

In this study, a series of cyclic triaxial tests was conducted on jointed rock specimens with a natural replicated joint surface (with

a $JRC = 11.51$ and $\phi = 51^\circ$) oriented at a mean dip angle of 60° . Tests were conducted at different confining pressures and cyclic deviatoric stress amplitudes. The samples were subjected to 10,000 loading-unloading cycles with a frequency of 8 Hz. At each level of

confining pressure, the applied cyclic deviatoric stress amplitude was increased incrementally until excessive deformation of the jointed rock specimen was observed. Most of the previous studies on rocks under cyclic loading conditions had focused on the deformation response and dynamic properties of intact rocks, and only a few studies are available related to the cyclic response of the jointed rocks. In comparison to the previous studies on rocks, this study focuses on the deformation behaviour and dynamic characteristics of jointed rocks with continuous penetrating joints, replicating a natural rough joint surface subjected to cyclic triaxial loading conditions. Moreover, the deformation behaviour and dynamic characteristics of jointed rocks under cyclic loadings in terms of residual axial deformation, resilient moduli, yielding stress, energy and damage evolution and damping characteristics were investigated and the main conclusions are drawn as follows:

- (1) For all the test conditions, the cyclic stress-strain hysteresis loops of the jointed rock specimens changed from sparse to dense with the increasing number of loading-unloading cycles.
- (2) There existed a critical cyclic deviatoric stress amplitude (i.e. critical dynamic deviatoric stress) beyond which yielding of the jointed rock specimens occurred. The ratio between critical dynamic deviatoric stress and the corresponding static peak deviatoric stress was in the range of 0.6–0.7. Moreover, the critical dynamic deviatoric stress showed an increasing trend with the confining pressure. The critical number of cycles corresponding to cyclic deviatoric stress amplitudes exceeding the critical dynamic deviatoric stresses was in the range of 10–20 under all the tested confining pressures.
- (3) At cyclic deviatoric stress amplitudes in excess of the critical dynamic deviatoric stress, the accumulated residual axial strains were extensively higher than those under lesser cyclic deviatoric stress amplitudes. Furthermore, with increasing confining pressure, the ultimate residual axial strains attained by the jointed rock specimens decreased. At cyclic deviatoric stress amplitudes in excess of the critical dynamic deviatoric stress threshold, upon inspection of the joint surface after applying the cyclic load, a considerable damage to the asperities could be observed, whereas no damage could be seen under lower cyclic deviatoric stress amplitudes.
- (4) At lower cyclic deviatoric stress amplitudes, the resilient moduli of the jointed rock specimens gradually degraded with number of cycles and tended to stabilise, whereas at cyclic deviatoric stress amplitudes in excess of the critical dynamic deviatoric stress threshold, the degradation of the resilient moduli with number of cycles was quite rapid during the initial loading cycles and stabilised during the rest of the loading cycles.
- (5) Both the dissipated energy density and damping ratio per load cycle values dramatically decreased during the initial loading cycles and then slightly recovered and gradually stabilised with further loading. A higher cyclic deviatoric stress amplitude led to higher initial dissipated energy density and initial damping ratio per load cycle values. Yet, when cyclic deviatoric stress amplitude exceeded the critical dynamic deviatoric stress, the initial dissipated energy density and initial damping ratio per load cycle values were significantly higher than that at lower cyclic deviatoric stress amplitudes. Moreover, the steady-state dissipated energy density and steady-state damping ratio per load cycle values

increased with increasing cyclic deviatoric stress amplitudes and decreasing confining pressures.

This study provides an important reference and quantifies variations of parameters such as permanent deformation, yielding stress, stiffness and damping ratio with field conditions. Design engineers can use the results of this study for more reliable predictions of the response of jointed rock subjected to cyclic loading and efficient and cost-effective solutions to curtail excessive deformation of structures built on or near jointed rock foundations subjected to cyclic loading from machine foundations, railway, road traffic loads and rock cutting.

Declaration of competing interest

The authors declare that they have no known competing financial interests or personal relationships that could have appeared to influence the work reported in this paper.

Acknowledgments

The first author would like to acknowledge the support and involvement provided for different aspects at various stages of this research project by Mr. Richard Berndt, Mr. Ritchie McLean, Mr. Duncan Best, Ms. Helen Jiang, Ms. Dilini Gunathilake, Mr. Mihimal Kadurugamuwa, Prof. Buddhima Indraratna, Dr. Vinod Jayan, Prof. Cholachat Rujikiatkamjorn and Prof. David McGloin.

References

- Abdellah, W.R., Ali, M.A., Boghdady, G.Y., Ibrahim, M.E., 2016. Evaluation of the effect of rock joints on the stability of underground tunnels. *J. Civil Eng. Architect. Res.* 3 (11), 1790–1799.
- ASTM D5311-13, 2013. Standard Test Method for Load Controlled Cyclic Triaxial Strength of Soil. ASTM International, West Conshohocken, PA, USA.
- Atapour, H., Moosavi, M., 2014. The influence of shearing velocity on shear behavior of artificial joints. *Rock Mech. Rock Eng.* 47 (5), 1745–1761.
- Attewell, P.B., Farmer, I.W., 1973. Fatigue behaviour of rock. *Int. J. Rock Mech. Min. Sci.* 10 (1), 1–9.
- Bagde, M.N., Petros, V., 2005a. Fatigue properties of intact sandstone samples subjected to dynamic uniaxial cyclical loading. *Int. J. Rock Mech. Min. Sci.* 42 (2), 237–250.
- Bagde, M.N., Petros, V., 2005b. Waveform effect on fatigue properties of intact sandstone in uniaxial cyclical loading. *Rock Mech. Rock Eng.* 38 (3), 169–196.
- Bagde, M.N., Petros, V., 2009. Fatigue and dynamic energy behaviour of rock subjected to cyclical loading. *Int. J. Rock Mech. Min. Sci.* 46 (1), 200–209.
- Belem, T., Souley, M., Homand, F., 2007. Modeling surface roughness degradation of rock joint wall during monotonic and cyclic shearing. *Acta Geotech* 2 (4), 227–248.
- Bian, X., Jiang, H., Cheng, C., Chen, Y., Chen, R., Jiang, J., 2014. Full-scale model testing on a ballastless high-speed railway under simulated train moving loads. *Soil Dynam. Earthq. Eng.* 66 (1), 368–384.
- Bieniawski, Z.T., 1967. Mechanism of brittle fracture of rock: Part I—theory of the fracture process. *Int. J. Rock Mech. Min. Sci.* 4 (4), 395–406.
- Brady, B.H., Brown, E.T., 1993. *Rock Mechanics: for Underground Mining*. Springer Science & Business Media.
- Brown, E., Hudson, J., 1973. Fatigue failure characteristics of some models of jointed rock. *Earthq. Eng. Struct. Dynam.* 2 (4), 379–386.
- Byerlee, J.D., 1970. The mechanics of stick-slip. *Tectonophysics* 9 (5), 475–486.
- Chen, T.C., Lin, M.L., Hung, J.J., 2004. Pseudostatic analysis of Tsao-Ling rockslide caused by Chi-Chi earthquake. *Eng. Geol.* 71 (1–2), 31–47.
- Craig, R.F., 2004. *Craig's Soil Mechanics*. CRC Press.
- Das, B.M., Ramana, G.V., 2011. *Principles of Soil Dynamics*. Cengage Learning.
- Ding, Z.D., Du, Y.G., Huang, J., Shi, C.H., 2014. Test study on dynamic deformation behavior of soft rock-concrete sample under cyclic loading. *Appl. Mech. Mater.* 501–504, 295–299.
- Fathi, A., Moradian, Z., Rivard, P., Ballivy, G., 2016. Shear mechanism of rock joints under pre-peak cyclic loading condition. *Int. J. Rock Mech. Min. Sci.* 83 (1), 197–210.
- Fuenkajorn, K., Phueakphum, D., 2010. Effects of cyclic loading on mechanical properties of Maha Sarakham salt. *Eng. Geol.* 112 (1–4), 43–52.

- Gong, L., Heitor, A., Indraratna, B., 2018. An approach to measure infill matric suction of irregular infilled rock joints under constant normal stiffness shearing. *J. Rock Mech. Geotech. Eng.* 10 (4), 653–660.
- Goodman, R.E., 1989. *Introduction to Rock Mechanics*. Wiley, New York, USA.
- Guo, S., Qi, S., 2015. Numerical study on progressive failure of hard rock samples with an unfilled undulate joint. *Eng. Geol.* 193 (1), 173–182.
- He, M.M., Zhang, Z.Q., Li, N., 2021. Experimental investigation and empirical model to determine the damping and shear stiffness properties of soft rock under multistage cyclic loading. *Soil Dynam. Earthq. Eng.* 147 (1), 106818.
- Hobbs, D., 1966. Scale model studies of strata movement around mine roadways. Apparatus, technique and some preliminary results. *Int. J. Rock Mech. Min. Sci.* 3 (2), 101–112.
- Huang, X., Haimson, B.C., Plesha, M.E., Qiu, X., 1993. An investigation of the mechanics of rock joints—Part I. Laboratory investigation. *Int. J. Rock Mech. Min. Sci.* 30 (3), 257–269.
- Huang, C.J., Yin, H.Y., Chen, C.Y., Yeh, C.H., Wang, C.L., 2007. Ground vibrations produced by rock motions and debris flows. *J. Geophys. Res. Earth Surf.* 112 (1), F02014.
- Hung, O., Coates, D.F., 1978. Deformability of joints and its relation to rock foundation settlements. *Can. Geotech. J.* 15 (2), 239–249.
- Hutson, R.W., Dowding, C.H., 1990. Joint asperity degradation during cyclic shear. *Int. J. Rock Mech. Min. Sci.* 27 (2), 109–119.
- Indraratna, B., 1990. Development and applications of a synthetic material to simulate soft sedimentary rocks. *Geotechnique* 40 (2), 189–200.
- Jafari, M.K., Hosseini, K.A., Pellet, F., Boulon, M., Buzzi, O., 2003. Evaluation of shear strength of rock joints subjected to cyclic loading. *Soil Dynam. Earthq. Eng.* 23 (7), 619–630.
- Jafari, M.K., Pellet, F., Boulon, M., Hosseini, K.A., 2004. Experimental study of mechanical behaviour of rock joints under cyclic loading. *Rock Mech. Rock Eng.* 37 (1), 3–23.
- Jahanian, H., Sadaghiani, M.H., 2015. Experimental study on the shear strength of sandy clay infilled regular rough rock joints. *Rock Mech. Rock Eng.* 48 (3), 907–922.
- Jia, C., Xu, W., Wang, R., Wang, W., Zhang, J., Yu, J., 2018. Characterisation of the deformation behavior of fine-grained sandstone by triaxial cyclic loading. *Construct. Build. Mater.* 162 (1), 113–123.
- Jibson, R.W., Harp, E.L., Schulz, W., Keefer, D.K., 2006. Large rock avalanches triggered by the M 7.9 Denali Fault, Alaska, earthquake of 3 November 2002. *Eng. Geol.* 83 (1–3), 144–160.
- Kou, M., Liu, X., Tang, S., Wang, Y., 2019. Experimental study of the prepeak cyclic shear mechanical behaviors of artificial rock joints with multiscale asperities. *Soil Dynam. Earthq. Eng.* 120 (1), 58–74.
- Lacy, H.S., Gould, J.P., 1985. Settlement from pile driving in sands. In: *Vibration Problems in Geotechnical Engineering*, pp. 152–173. ASCE.
- Lee, H.S., Park, Y.J., Cho, T.F., You, K.H., 2001. Influence of asperity degradation on the mechanical behavior of rough rock joints under cyclic shear loading. *Int. J. Rock Mech. Min. Sci.* 38 (7), 967–980.
- Li, N., Chen, W., Zhang, P., 2001a. Strength properties of the jointed rock mass medium under dynamic cyclic loading. *Prog. Nat. Sci.* 11 (3), 197–201.
- Li, N., Chen, W., Zhang, P., Swoboda, G., 2001b. The mechanical properties and a fatigue-damage model for jointed rock masses subjected to dynamic cyclical loading. *Int. J. Rock Mech. Min. Sci.* 38 (7), 1071–1079.
- Li, T., Pei, X., Wang, D., Huang, R., Tang, H., 2019. Nonlinear behavior and damage model for fractured rock under cyclic loading based on energy dissipation principle. *Eng. Fract. Mech.* 206 (1), 330–341.
- Liang, W., Zhang, C., Gao, H., Yang, X., Xu, S., Zhao, Y., 2012. Experiments on mechanical properties of salt rocks under cyclic loading. *J. Rock Mech. Geotech. Eng.* 4 (1), 54–61.
- Liu, Y., Dai, F., 2021. A review of experimental and theoretical research on the deformation and failure behavior of rocks subjected to cyclic loading. *J. Rock Mech. Geotech. Eng.* 13 (5), 1203–1230.
- Liu, E., He, S., 2012. Effects of cyclic dynamic loading on the mechanical properties of intact rock samples under confining pressure conditions. *Eng. Geol.* 125 (1), 81–91.
- Liu, M., Liu, E., 2017. Dynamic mechanical properties of artificial jointed rock samples subjected to cyclic triaxial loading. *Int. J. Rock Mech. Min. Sci.* 98 (1), 54–66.
- Liu, E., He, S., Xue, X., Xu, J., 2011. Dynamic properties of intact rock samples subjected to cyclic loading under confining pressure conditions. *Rock Mech. Rock Eng.* 44 (5), 629–634.
- Liu, E., Huang, R., He, S., 2012. Effects of frequency on the dynamic properties of intact rock samples subjected to cyclic loading under confining pressure conditions. *Rock Mech. Rock Eng.* 45 (1), 89–102.
- Liu, Y., Dai, F., Fan, P., Xu, N., Dong, L., 2017. Experimental investigation of the influence of joint geometric configurations on the mechanical properties of intermittent jointed rock models under cyclic uniaxial compression. *Rock Mech. Rock Eng.* 50 (6), 1453–1471.
- Liu, Y., Dai, F., Dong, L., Xu, N., Feng, P., 2018a. Experimental investigation on the fatigue mechanical properties of intermittently jointed rock models under cyclic uniaxial compression with different loading parameters. *Rock Mech. Rock Eng.* 51 (1), 47–68.
- Liu, Y., Dai, F., Feng, P., Xu, N.W., 2018b. Mechanical behavior of intermittent jointed rocks under random cyclic compression with different loading parameters. *Soil Dynam. Earthq. Eng.* 113 (1), 12–24.
- Liu, H., Gao, K., Zhu, X., 2021a. Experimental study on dynamic fatigue properties of dolomite samples under triaxial multi-level cyclic loading. *Bull. Eng. Geol. Environ.* 80 (1), 551–565.
- Liu, M., Liu, E., Feng, J., Zheng, Q., Fu, J., Luo, W., 2021b. Dynamic mechanical properties of jointed soft rock samples subjected to cyclic triaxial loading: a FEM-DEM-based study. In: *IOP Conference Series: Earth and Environmental Science*, vol. 676. IOP Publishing, 012066.
- Ma, L.J., Liu, X.Y., Wang, M.Y., et al., 2013. Experimental investigation of the mechanical properties of rock salt under triaxial cyclic loading. *Int. J. Rock Mech. Min. Sci.* 62, 34–41.
- Martin, C.D., Chandler, N.A., 1994. The progressive fracture of Lac du Bonnet granite. *Int. J. Rock Mech. Min. Sci.* 31 (6), 643–659.
- Momeni, A., Karakus, M., Khanlari, G.R., Heidari, M., 2015. Effects of cyclic loading on the mechanical properties of a granite. *Int. J. Rock Mech. Min. Sci.* 100 (77), 89–96.
- Monismith, C.L., Ogawa, N., Freeme, C.R., 1975. Permanent deformation characteristics of subgrade soils due to repeated loading. *Transport. Res. Rec.* 537 (1), 1–17.
- Ng, C.W.W., Liu, G.B., Li, Q., 2013. Investigation of the long-term tunnel settlement mechanisms of the first metro line in Shanghai. *Can. Geotech. J.* 50 (6), 674–684.
- Nie, R., Li, Y., Leng, W., Mei, H., Dong, J., Chen, X., 2020. Deformation characteristics of fine-grained soil under cyclic loading with intermittence. *Acta Geotech* 15 (1), 3041–3054.
- Niktabar, S.M., Rao, K.S., Shrivastava, A.K., 2017. Effect of rock joint roughness on its cyclic shear behavior. *J. Rock Mech. Geotech. Eng.* 9 (6), 1071–1084.
- Peillage, W.H., Fatahi, B., Rasekh, H., 2022. Experimental investigation for vibration characteristics of jointed rocks using cyclic triaxial tests. *Soil Dynam. Earthq. Eng.* 160 (1), 107377.
- Peng, K., Zhou, J., Zou, Q., Zhang, J., Wu, F., 2019. Effects of stress lower limit during cyclic loading and unloading on deformation characteristics of sandstones. *Construct. Build. Mater.* 217 (1), 202–215.
- PLAXIS, 2022. *PLAXIS 3D Material Models Manual*. Bentley Systems International Limited.
- Prakash, S., 1981. *Soil Dynamics*. McGraw Hill, New York, USA.
- Premadasa, W.N., 2013. *The Influence of Infill Saturation on the Shear Strength of Soil-Infilled Rock Joints*. PhD Thesis. University of Wollongong, Wollongong, Australia.
- Prost, G.L., 1988. Jointing at rock contacts in cyclic loading. *Int. J. Rock Mech. Min. Sci.* 25 (5), 263–272.
- Qi, S., Xu, Q., Zhang, B., Zhou, Y., Lan, H., Li, L., 2011. Source characteristics of long runout rock avalanches triggered by the 2008 Wenchuan earthquake, China. *J. Asian Earth Sci.* 40 (4), 896–906.
- Rainer, J.H., 1982. Effect of vibrations on historic buildings: an overview. *Bull. Assoc. Preserv. Technol.* 14 (1), 2–10.
- Rosenblad, J.L., 1971. *Geomechanical Model Study of the Failure Modes of Jointed Rock Masses*. PhD Thesis. University of Illinois at Urbana-Champaign, II, USA.
- Sheng, X., Jones, C.J.C., Thompson, D.J., 2006. Prediction of ground vibration from trains using the wavenumber finite and boundary element methods. *J. Sound Vib.* 293 (3–5), 575–586.
- Shi, C.H., Lei, M.F., Peng, L.M., 2014. Accumulated deformation behavior and computational model of water-rich mudstone under cyclic loading. *Rock Mech. Rock Eng.* 47 (4), 1485–1491.
- Sinha, U.N., Singh, B., 2000. Testing of rock joints filled with gouge using a triaxial apparatus. *Int. J. Rock Mech. Min. Sci.* 37 (6), 963–981.
- Song, S., Liu, X., Tan, Y., Fan, D., Ma, Q., Wang, H., 2020. Study on failure modes and energy evolution of coal-rock combination under cyclic loading. *Shock Vib.* 2020 (1), 1–16.
- Stimpson, B., 1970. Modelling materials for engineering rock mechanics. *Int. J. Rock Mech. Min. Sci.* 7 (1), 77–121.
- Tao, Z.Y., Mo, H.H., 1990. An experimental study and analysis of the behaviour of rock under cyclic loading. *Int. J. Rock Mech. Min. Sci.* 27 (1), 51–56.
- Tse, R., Cruden, D.M., 1979. Estimating joint roughness coefficients. *Int. J. Rock Mech. Min. Sci.* 16 (5), 303–307.
- Vaneghi, R.G., Ferdosi, B., Okoth, A.D., Kuek, B., 2018. Strength degradation of sandstone and granodiorite under uniaxial cyclic loading. *J. Rock Mech. Geotech. Eng.* 10 (1), 117–126.
- Waltham, A.C., Swift, G.M., 2004. Bearing capacity of rock over mined cavities in Nottingham. *Eng. Geol.* 75 (1), 15–31.
- Wang, Z., Li, S., Qiao, L., Zhao, J., 2013. Fatigue behavior of granite subjected to cyclic loading under triaxial compression condition. *Rock Mech. Rock Eng.* 46 (6), 1603–1615.
- Wang, K., Zhuang, Y., 2021. Characterising the permanent deformation response-behavior of subgrade material under cyclic loading based on the shakedown theory. *Construct. Build. Mater.* 311 (1), 125325.
- Xiao, J.Q., Ding, D.X., Xu, G., Jiang, F.L., 2009. Inverted S-shaped model for nonlinear fatigue damage of rock. *Int. J. Rock Mech. Min. Sci.* 46 (3), 643–648.
- Xiao, J.Q., Ding, D.X., Jiang, F.L., Xu, G., 2010. Fatigue damage variable and evolution of rock subjected to cyclic loading. *Int. J. Rock Mech. Min. Sci.* 47 (3), 461–468.

- Xie, H., Wang, J.A., Xie, W.H., 1997. Fractal effects of surface roughness on the mechanical behavior of rock joints. *Chaos, Solit. Fractals* 8 (2), 221–252.
- Yang, Y., Duan, H., Xing, L., Ning, S., Lv, J., 2018. Fatigue characteristics of limestone under triaxial compression with cyclic loading. *Adv. Civ. Eng.* 2018 (1), 8681529.
- Yang, Y., Ju, Y., Li, F., Gao, F., Sun, H., 2016. The fractal characteristics and energy mechanism of crack propagation in tight reservoir sandstone subjected to triaxial stresses. *J. Nat. Gas Sci. Eng.* 32 (1), 415–422.
- Yasuhara, K., Murakami, S., Toyota, N., Hyde, A.F., 2001. Settlements in fine-grained soils under cyclic loading. *Soils Found.* 41 (6), 25–36.
- Zhang, M., Meng, Q., Liu, S., 2017. Energy evolution characteristics and distribution laws of rock materials under triaxial cyclic loading and unloading compression. *Adv. Mater. Sci. Eng.* 2017 (1), 5471571.
- Zhang, C.L., Jiang, G.L., Su, L.J., Liu, W.M., 2018. Dynamic behaviour of weathered red mudstone in Sichuan (China) under triaxial cyclic loading. *J. Mt. Sci.* 15 (8), 1789–1806.
- Zhang, X., Jiang, Q., Kulatilake, P.H.S.W., Xiong, F., Yao, C., Tang, Z., 2019. Influence of asperity morphology on failure characteristics and shear strength properties of rock joints under direct shear tests. *Int. J. GeoMech.* 19 (2), 04018196.
- Zheng, B., Qi, S., 2016. A new index to describe joint roughness coefficient (JRC) under cyclic shear. *Eng. Geol.* 212, 72–85.
- Zheng, Q., Liu, E., Sun, P., Liu, M., Yu, D., 2020a. Dynamic and damage properties of artificial jointed rock samples subjected to cyclic triaxial loading at various frequencies. *Int. J. Rock Mech. Min. Sci.* 128 (1), 104243.
- Zheng, Q., Liu, E., Yu, D., Liu, M., 2020b. Fatigue and damage properties of non-consecutive jointed mudstone samples subjected to cyclic triaxial loading. *Bull. Eng. Geol. Environ.* 79 (5), 2467–2481.



Behzad Fatahi is an award-winning engineer and internationally recognised academic for his work in the field of geomechanics and soil-structure interaction. He has been working at the frontier of new infrastructure and building technologies and solutions, in particular, systems that will make infrastructure (e.g. roads, railways, pipelines, large energy storage tanks) and buildings safer and more resilient. He is currently Head of Discipline (Geotechnical and Transport Engineering) and an Associate Professor of Civil Engineering in the School of Civil and Environmental Engineering at the University of Technology Sydney (UTS) in Australia. Dr. Fatahi has been involved in design and construction in many major infrastructure projects in Australia and overseas. Behzad is a

Chartered Professional Engineer (Civil, Geotechnical and Structural Engineering Colleges) and Fellow of Engineers Australia. He was named Australasia Young Railway Engineer of the Year by Engineers Australia and the Railway Technical Society of Australasia. Behzad was also awarded with the first prize at the Young Geotechnical Professional Night, which is a prestigious geotechnical engineering award from the Australian Geomechanics Society. He has supervised 19 PhD candidate to completion as the principal supervisor and have published more than 250 peer-reviewed technical papers in top journals and conference proceedings in the fields of Civil, Geotechnical and Structural Engineering. His PhD student, Ms. Waranga Habaraduwa Peellage (1st author of this paper) was the recipient of the Best Oral Presentation Award in the 2022 Transport Research Association of New South Wales (TRANSW) Symposium.